Reconstructing the kinematic evolution of curved mountain belts: Internal strain patterns in the Wyoming salient, Sevier thrust belt, U.S.A.

Adolph Yonkee[1,†] and Arlo Brandon Weil[2]
[1]*Department of Geosciences, Weber State University, Ogden, Utah 84408, USA*
[2]*Department of Geology, Bryn Mawr College, Bryn Mawr, Pennsylvania 19010, USA*

ABSTRACT

Analyses of mesoscopic structural and strain patterns in red beds of the Triassic Ankareh Formation and limestones of the Jurassic Twin Creek Formation, in concert with complementary paleomagnetic studies, constrain the three-dimensional kinematic evolution of curved fold-and-thrust systems in the Wyoming salient of the Sevier thrust belt. Spaced cleavage, fracture and vein networks, minor folds, and minor faults in limestones and red beds accommodated early layer-parallel shortening (LPS) concentrated in front of the growing thrust wedge, along with minor strike-parallel extension and wrench shear related to the development of orogenic curvature. Strain, estimated using mass balance relations for cleavage seams, crinoid ossicles in bioclastic limestone, and reduction spots in red beds, displays systematic regional patterns. Principal shortening directions are subperpendicular to structural trend around the salient, reflecting a combination of primary curvature and secondary rotation of early LPS fabrics. LPS magnitudes vary from <5% in central parts of the frontal Hogsback thrust system, where cleavage is absent, to 10%–30% in the more interior Crawford thrust system, where cleavage intensity is moderate to strong; strain also increases toward the salient ends. Internal strain is a significant component of total deformation and should be considered when restoring cross sections. Strain patterns are consistent with a kinematic model involving curved fault slip and differential shortening that produced progressive secondary curvature during thrusting.

INTRODUCTION

Map-view curvature is a fundamental feature of most ancient and active mountain belts, and has been the focus of study for over a century (e.g., Suess, 1909; Hobbs, 1914; Carey, 1955; Butler et al., 1995; Muttoni et al., 1998; Schill et al., 2002; Marshak, 2004; Sussman et al., 2004; Weil and Sussman, 2004). Although analog and numerical models have identified potential factors for developing orogenic curvature, such as initial thickness variations of sedimentary prisms, strength changes along detachment horizons, shape and motion of indentors, foreland buttress effects, and superposed deformation (Marshak et al., 1992; Ferrill and Groshong, 1993; Macedo and Marshak, 1999; Lickorish et al., 2002), key processes responsible for curvature formation in most mountain belts remain obscure. In order to decipher these processes and better understand the evolution of orogenic systems, kinematic histories must first be determined.

The kinematic history of a mountain belt is recorded in the temporal evolution of its three-dimensional displacement field, which is composed of: bulk translation, bulk rotation, and internal strain (Fig. 1). Quantification of deformation is scale-dependent, and we consider bulk translation to be produced by slip on major faults, horizontal- and vertical-axis rotations to be produced by large-scale folds and motion of coherent blocks, and internal strain to be accommodated by mesoscopic structures (cleavage, fracture and vein networks, minor folds, and minor faults) and grain-scale fabrics. The final deformed state yields a finite displacement field that may arise by a variety of deformation paths. Thus, it is critical to determine timing relations, evaluate incremental deformation markers, and utilize spatial variations in strain to constrain deformation paths.

Bulk translation is commonly estimated from apparent offset of beds across major faults on cross sections constructed approximately perpendicular to structural trend (e.g., Dixon, 1982; Kley and Monaldi, 1998). Such sections imply radial thrust slip around curved mountain belts, which would produce major strike-parallel (tangential) extension; however, major extension is generally not observed. Alternatively, translation may be accompanied by vertical-axis rotations along curved slip paths oblique to structural trend, which would result in out-of-plane motions not accounted for on classically constructed cross sections (Hindle and Burkhard, 1999; Pueyo et al., 2004). Better estimates of translation can be made by determining true offset of piercing points across faults, incorporating rotation data into restorations (Pueyo et al., 2004), and analyzing fault-slip lineations (Allerton, 1998). Moreover, most cross sections only show bulk shortening from large-scale faults and folds (e.g., Dahlstrom, 1969; Wilkerson and Dicken, 2001), whereas contributions from internal strain are generally not included, which may result in underestimates of cumulative shortening (Mitra, 1994). Only by including strain and vertical-axis rotation data, can orogenic wedges be accurately restored.

Orientations and magnitudes of internal strain are typically evaluated by detailed analysis of mesoscopic structures and grain-scale fabrics (e.g., Ramsay, 1981; Mitra, 1994; Hogan and Dunne, 2001; Kwon and Mitra, 2004). Although external thrust sheets are often assumed to have only limited strain, spaced cleavage and minor faults may accommodate significant internal shortening at shallow levels (Mitra and Yonkee, 1985; Sans et al., 2003). Many thrust sheets are lithologically and rheologically layered, such that strain can be factored into components of layer-parallel shortening (LPS), tangential (strike-parallel) extension, layer-parallel shear, and wrench shear (Fig. 1). LPS fabrics that form early in the deformation history are widespread in most orogenic belts and provide key constraints for kinematic models (e.g., Geiser and Engelder, 1983; Ong et al., 2007). Tangential extension (or shortening) parallel to structural trend may also be locally important, especially in areas of orogenic curvature (e.g., Ries and Shackleton, 1976; Ferrill and Groshong, 1993; Marshak, 1988, 2004).

Distributions and magnitudes of vertical-axis rotations are primarily determined by paleomagnetic analysis, which provides the most robust means of distinguishing between secondary rotation and primary curvature (e.g.,

[†]E-mail: ayonkee@weber.edu.

GSA Bulletin; January/February 2010; v. 122; no. 1/2; p. 24–49; doi: 10.1130/B26484.1; 23 figures; Data Repository item 2009097.

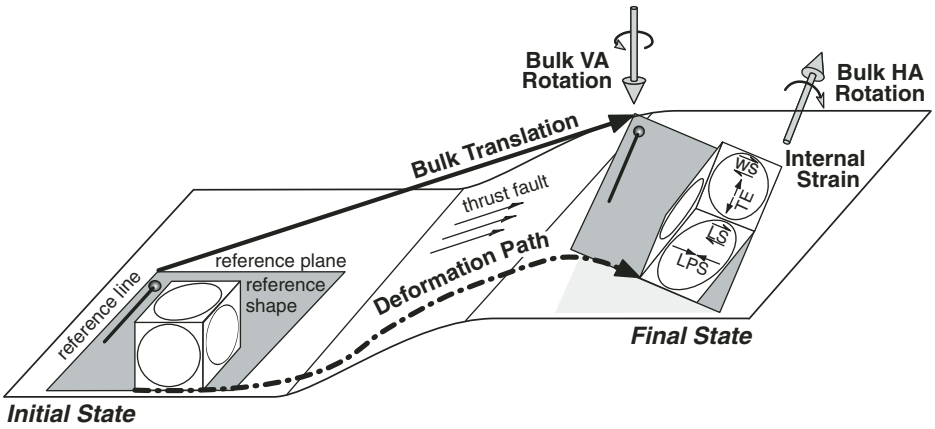

Deformation Components	*Structural Features*
Bulk Translation	large-scale thrust faults
Bulk Rotation	
Components	
HA—horizontal axis	large-scale folds
VA—vertical axis	coherent block rotations and regional bending
Internal Strain	
Components	
LPS—layer-parallel shortening	spaced cleavage, minor folds, minor faults,
TE—tangential extension	veins, grain-scale fabrics
LS—layer-parallel shear	
WS—wrench shear	

Figure 1. The total displacement field includes bulk translation, bulk rotation, and internal strain. Translation is produced by slip along large-scale faults. Horizontal-axis (HA) rotation produces large-scale folds and tilted bedding. Vertical-axis (VA) rotation is related to movement of coherent blocks and can be estimated from restoration of paleomagnetic vectors. Internal strain, including components of layer-parallel shortening (LPS), tangential extension (TE), layer-parallel shear (LS), and wrench shear (WS), is recorded by mesoscopic structures and grain-scale fabrics. The final deformed state can be arrived at by various deformation paths.

Van der Voo and Channell, 1980; Schwartz and Van der Voo, 1983; McCaig and McClelland, 1992; Butler et al., 1995; Stamatakos et al., 1996; Speranza et al., 1997; Weil et al., 2000, 2001; Conder et al., 2003). Due to protracted deformation and structural complications found in most orogens, care is needed to accurately determine timing of magnetization and restoration paths. Although strain fabrics have also been used to estimate vertical-axis rotations by assuming initial shortening directions, different studies have reached varying interpretations. For example, changes in calcite twin strain directions around the Cantabrian-Asturian arc roughly match rotations determined from paleomagnetic analysis (Kollmeier et al., 2000; Weil et al., 2000). In comparison, strain directions in the Jura arc do not correspond directly to paleomagnetically measured rotations and are locally oblique to regional structural trend (Hindle and Burkhard, 1999). Such varied results indicate the importance of utilizing multiple data sets to understand the evolution of orogenic curvature (Gray and Stamatakos, 1997; Bayona et al., 2003; Hnat et al., 2008).

Curved mountain belts can be broadly described as primary arcs, progressive arcs, or secondary oroclines based on their kinematic histories and timing of curvature acquisition (Weil and Sussman, 2004). Primary arcs begin with initial curvature prior to major deformation, do not experience secondary rotations, and can form by uniform or radial slip (Fig. 2, models 1 and 2). Although both of these models have no vertical-axis rotation, radial slip produces major tangential extension, whereas uniform slip has no additional extension. Progressive arcs develop increasing curvature during orogenic evolution, and can form by curved slip during divergent thrust emplacement or by parallel slip during differential shortening (Fig. 2, models 3 and 4). Although both models have synthrusting vertical-axis rotation, curved slip produces fault-slip lineations with variable trends and minor tangential extension, whereas parallel slip produces lineations with consistent trend and minor wrench shear. Secondary oroclines start as originally linear belts that are bent into curved shapes during a subsequent phase of wrenching or bending (Fig. 2, models 5 and 6). Orocline models involve younger rotation and strain superimposed on older deformation fabrics. Each of these models predicts different kinematic histories that can be compared with structural and paleomagnetic data from mountain belts. Ultimately, kinematic patterns reflect the mechanical processes responsible for development of orogenic curvature.

In order to better understand the three-dimensional kinematic evolution and processes that produce orogenic curvature, we have undertaken an integrated structural and paleomagnetic study of the Wyoming salient of the Sevier thrust belt (Fig. 3). Results of our studies are presented in this paper, which focuses on patterns of internal strain, followed by a complementary paper on vertical-axis rotation patterns determined by paleomagnetic studies (Weil et al., 2009). By integrating multiple techniques, we reduce the limitations of individual data sets. Cumulatively, these papers will address the following questions:

1. How are internal strain and vertical-axis rotation related to evolution of orogenic curvature?
2. What are the consequences of incorporating strain and rotation data into restorations of fold-and-thrust belts?
3. What processes were most important in developing curvature in the Wyoming salient, and how can these processes be best identified in other orogens?

The Wyoming salient is an excellent location to study orogenic curvature because: (1) thrust and fold traces display systematic regional bends; (2) timing relations of thrust systems are well constrained (e.g., Wiltschko and Dorr, 1983; DeCelles, 1994); (3) much of the region is covered by geologic maps at scales ≤1:100,000 (e.g., Mansfield, 1927; Oriel and Platt, 1980, and references therein; Bryant, 1992); (4) seismic and drill-hole data provide key constraints for constructing cross sections (e.g., Dixon, 1982; Royse, 1993); (5) previous studies have documented locally significant vertical-axis rotations and internal strain (e.g., Grubbs and Van der Voo, 1976; Mitra, 1994); and (6) a variety of processes appears to have been important in the evolution of the salient, including buttressing and variations in stratigraphic thickness (e.g., Beutner, 1977; Paulsen and Marshak, 1999).

GEOLOGIC SETTING

The Sevier thrust belt lies in the eastern margin of the North American Cordillera, and is characterized by folds and thrust faults that

shortened and translated miogeoclinal rocks overall eastward toward the craton during the Early Cretaceous to Paleogene (Armstrong and Oriel, 1965; Armstrong, 1968; Blackstone, 1977; Royse, 1993; DeCelles, 2004). The belt is divided into a number of salients (Lawton et al., 1994), including the Wyoming salient, which is bounded on the north and south by the basement-cored Gros Ventre and Uinta foreland uplifts (Fig. 3).

Major thrust systems in the Wyoming salient, from west to east, are the: Willard (made up of the Willard, Paris, and Meade thrusts), Crawford (and associated fold train), Absaroka (and associated imbricates), and Hogsback (made up of the Hogsback, Darby, Prospect, and Granite Creek thrusts) (Fig. 3). Major thrust and fold traces display over 90° of regional curvature in map view, from NW trends in the northern part of the salient, to NE trends in the southern part, with additional curvature near oblique thrust ramps and transfer zones. Spacing between major thrusts is approximately constant within the central part of the salient, but spacing locally

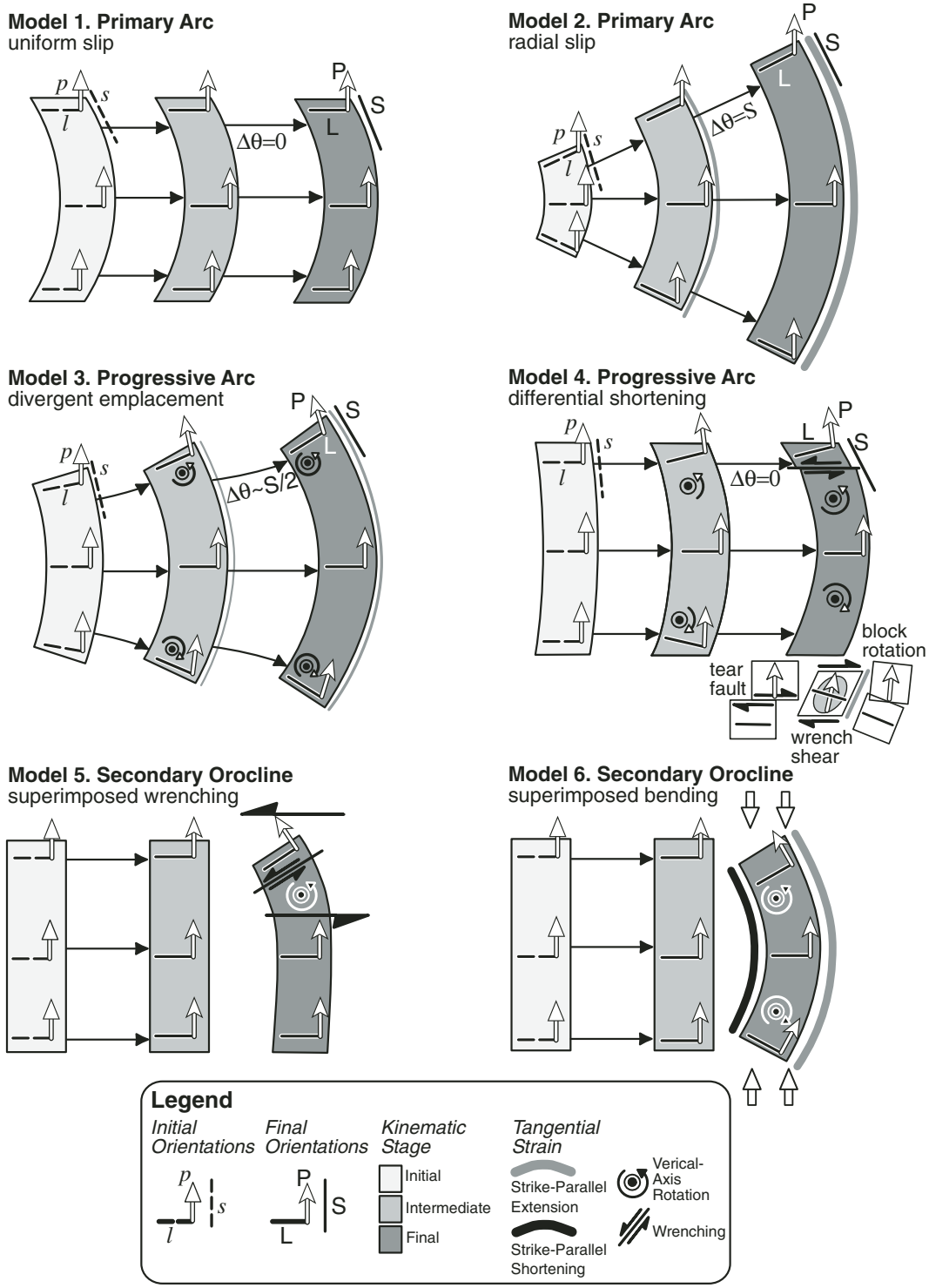

Figure 2. Simplified kinematic models for (1) primary arc with uniform slip, (2) primary arc with radial slip, (3) progressive arc with curved slip during divergent thrust emplacement, (4) progressive arc with parallel slip during differential thrust shortening, (5) secondary orocline with superimposed wrenching, and (6) secondary orocline with superimposed bending. Each model predicts different patterns of vertical-axis rotations recorded by paleomagnetic vectors (*p*/P), changes in structural trend (*s*/S), changes in layer-parallel shortening directions (*l*/L), varying tangential strain, and different trends of fault slip (θ). Insets for model 4 illustrate ways to accommodate differential shortening by tear faults, distributed wrench shear, and local block rotations.

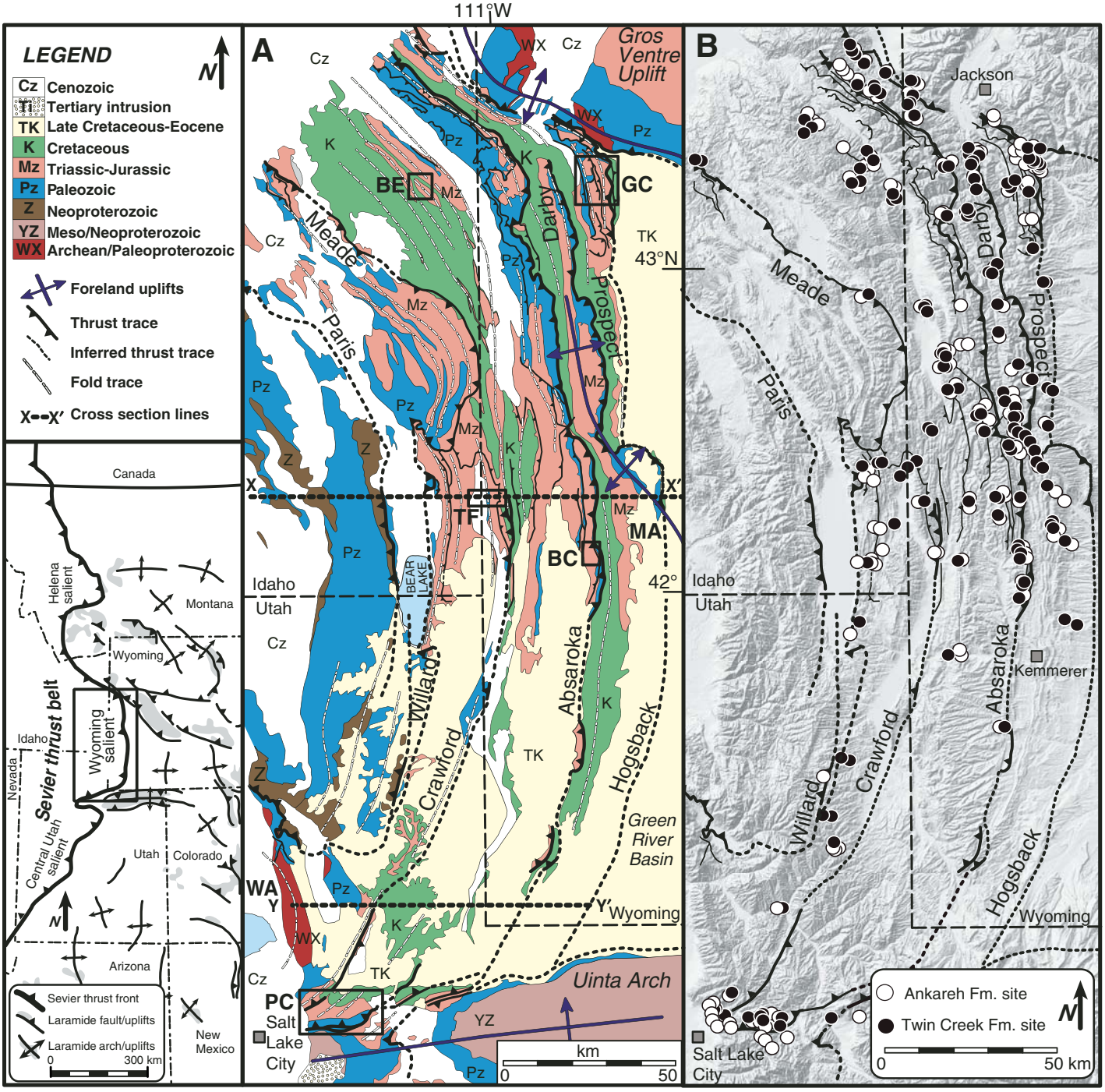

Figure 3. (A) Generalized geologic map of the Wyoming salient. Major thrusts and associated folds display regional curvature from NW trends in the northern part to NE trends in the southern part of the salient. Labeled features are: BE—Big Elk anticline, BC—Beaver Creek area, GC—Granite Creek area, MA—Moxa Arch, PC—Parleys Canyon area, TF—Thomas Fork anticline, and WA—Wasatch anticlinorium. Locations of cross-sections X-X′ and Y-Y′ shown in Figure 4 are indicated. Inset regional map shows major salients of Sevier thrust belt and relations to Laramide foreland uplifts. The Wyoming salient is bounded on the north and south by the Gros Ventre Uplift and Uinta Arch. (B) Digital elevation map of the Wyoming salient showing distribution of sampled site locations in the Twin Creek Formation (black circles) and Ankareh Formation (white circles). Sites are widely distributed along and across strike of the Crawford, Absaroka, and Hogsback thrust systems.

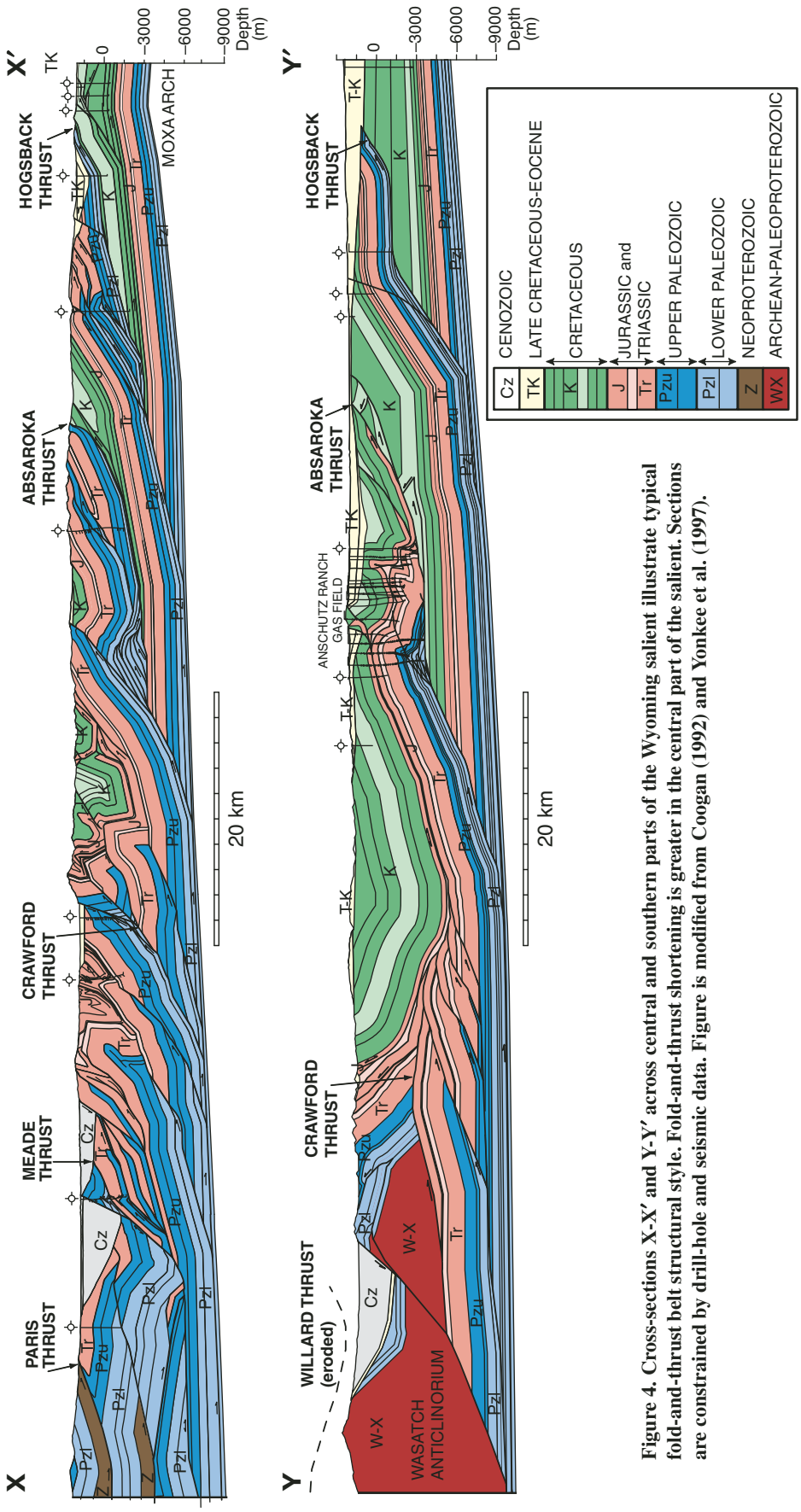

Figure 4. Cross-sections X-X′ and Y-Y′ across central and southern parts of the Wyoming salient illustrate typical fold-and-thrust belt structural style. Fold-and-thrust shortening is greater in the central part of the salient. Sections are constrained by drill-hole and seismic data. Figure is modified from Coogan (1992) and Yonkee et al. (1997).

decreases at the northern and southern ends of the salient where the thrust belt impinges on foreland uplifts. Synorogenic deposits and thermochronologic data record an overall foreland propagating (west to east) sequence of thrusts, from the Early Cretaceous Willard system, to the middle Cretaceous Crawford system, to the mostly Late Cretaceous Absaroka system, to the early Paleogene Hogsback system (Dorr et al., 1977; Wiltschko and Dorr, 1983; Burtner and Nigrini, 1994; DeCelles, 1994, 2004). Minor reactivation of more internal thrust sheets, limited out-of-sequence thrusts, and uplift over deep basement ramps also accompanied development of the orogenic wedge and helped maintain critical taper (Coogan, 1992; DeCelles and Mitra, 1995).

Cross sections of the salient show typical thin-skinned fold-and-thrust structures that are constrained by seismic and drill-hole data (Fig. 4) (Royse et al., 1975; Dixon, 1982; Lammerson, 1982; Coogan, 1992; Royse, 1993; Yonkee et al., 1997). Frontal thrusts display typical ramp-flat geometries and have a common basal décollement in Cambrian shale. Underlying basement is not incorporated into the frontal thrust sheets, but it becomes involved in thrusting farther west in the Wasatch anticlinorium (WA in Figs. 3A and 4B; Schirmer, 1988; Yonkee, 1992). Basement is deformed in adjacent Laramide foreland uplifts, including the Gros Ventre Range, Uinta Arch, and Moxa Arch (Fig. 3A), which interacted with frontal thrusts. Fold-and-thrust shortening is greatest in the central part of the Wyoming salient and decreases toward the salient ends. Fault slip was overall eastward in central parts of the salient, but was oblique to structural trend near the salient ends.

Thrust sheets in the Wyoming salient display systematic suites of mesoscopic to microscopic structures that accommodated internal strain, including spaced cleavage, fracture and vein networks, minor folds, and minor faults (Crosby, 1969; Mitra and Yonkee, 1985; Craddock et al., 1988; Protzman and Mitra, 1990; Craddock, 1992; Mitra, 1994). Large parts of frontal thrust sheets have consistent strain patterns, with widespread LPS and minor tangential extension, such that strain characteristics can be projected and utilized in constructing balanced sections (Mitra, 1994). Strain patterns, however, are more complex at the salient ends (Bradley and Bruhn, 1988), near oblique ramps (Apotria, 1995), and in more internal thrust sheets (McNaught and Mitra, 1996; Yonkee, 2005).

Vertical-axis rotations have been interpreted from paleomagnetic studies within parts of the salient (Grubbs and Van der Voo, 1976; Schwartz and Van der Voo, 1984; McWhinnie et al., 1990). However, inconsistencies exist in

interpretations, partly due to limited sampling. By completing regional sampling that builds on previous work, integrating strain and paleomagnetic data, and conducting statistical analyses, we have developed a robust kinematic model for the Wyoming salient.

ANALYSIS OF INTERNAL STRAIN

Our studies were focused on two lithologies: (1) limestones of the Jurassic Twin Creek Formation; and (2) red beds of the Triassic Ankareh Formation. Both formations display consistent patterns of mesoscopic structures, contain strain markers, and carry interpretable paleomagnetic components. Structural data and paleomagnetic samples were collected for 154 sites within the Ankareh Formation, and for 144 sites plus 15 nearby subsites in the Twin Creek Formation (Fig. 3B). Site locations were chosen to provide wide spatial coverage within the Crawford, Absaroka, and Hogsback systems where these formations are well exposed. Additional detailed surveys were completed for individual large-scale folds and transfer zones to evaluate timing relations and structural complications.

At each study site, orientations of bedding and mesoscopic structures were measured and statistically analyzed. Sites in the Twin Creek Formation containing *Pentacrinus* ossicles were analyzed to estimate bed-parallel strain, and sites in the Ankareh Formation containing reduction spots were analyzed to estimate three-dimensional finite strain. Structural styles of the Twin Creek and Ankareh Formations are first described, orientations of mesoscopic structures are then analyzed, results of finite strain analysis are presented, and finally correlations between curvature and strain fabrics are quantified. Results of paleomagnetic analysis are presented in the accompanying paper by Weil et al. (2009).

Structural Style

The Twin Creek Formation consists mostly of variably argillaceous micritic limestone, with minor bioclastic and oolitic limestone (Imlay, 1967). Red beds of the Ankareh Formation consist mostly of quartzose to arkosic, variably calcareous mudstone to sandstone (Kummel, 1954). Mesoscopic structures in both formations include cleavage, fracture and vein networks, minor faults, and minor folds. *Pentacrinus* ossicles in bioclastic limestone and reduction spots in red beds vary from undeformed in central parts of the frontal Hogsback system to elliptical in the more interior Crawford system (Protzman and Mitra, 1990; Mitra, 1994).

Cleavage in the Twin Creek Formation is defined by close-spaced partings at high angles to bedding in more deformed micritic limestone, recording early LPS (Fig. 5A). Oolitic limestone and less-deformed areas have wider-spaced tectonic stylolites. Local cleavage refraction reflects minor bed-parallel shear. Microscopically, cleavage is defined by seams enriched in clay and quartz, which bound less-deformed microlithons (Fig. 5B). Seams and tectonic stylolites truncate fossil fragments and ooids (Fig. 5C) and were formed mostly by dissolution of calcite.

Cleavage in the Ankareh Formation is defined by anastomosing partings at high angles to bedding (Fig. 6A). Cleavage is better developed in calcareous mudstone compared to quartzose sandstone. Microscopically, cleavage is defined by discontinuous seams enriched in clay and hematite, which formed mostly by dissolution of calcite and quartz (Fig. 6B). Cleavage is approximately perpendicular to the shortening direction defined by shape fabrics of reduction spots in the Ankareh Formation and deformed *Pentacrinus* ossicles in the Twin Creek Formation. Cleavage intensity in calcareous mudstone and micritic limestone varies from moderate to strong in the Crawford system to absent in central parts of the Hogsback system, although intensity increases toward the salient ends.

Veins are widely developed in the Twin Creek Formation. A dominant set subperpendicular to structural trend (cross-strike set) accommodated tangential extension (Figs. 5D). Cross-strike veins are locally grouped into en echelon arrays and rotated into sigmoidal shapes, recording wrench shear parallel to array boundaries. Shearing and small-scale block rotation of early fabrics, followed by continued LPS and extension, produced locally acute subsets of cleavage and cross-strike veins that provide a record of incremental deformation. Veins parallel to bedding accommodated minor extension down the dip of cleavage. Veins both crosscut and are dissolved along cleavage seams, recording overlapping development.

Fractures and veins are widely developed in sandstone of the Ankareh Formation, including two regionally consistent sets: one set at high angles to bedding and subparallel to structural trend (high-angle set); and a second set subperpendicular to structural trend (cross-strike set). The high-angle set is interpreted to reflect fracturing along preexisting LPS fabrics during unloading, based on having similar orientations as cleavage in mudstone. Some fractures, however, may have formed during large-scale folding and thrusting. Cross-strike fractures and associated veins record minor extension subparallel to structural trend. Some sites display subsets of high-angle and cross-strike fractures that are at acute (~10°–30°) angles to each other. Such subsets are interpreted to record local block rotations or stress changes during progressive deformation, similar to patterns in the Twin Creek Formation. Additional fracture sets are locally developed oblique to structural trend, especially near oblique ramps.

Minor faults, which grade into shear veins, define two broad groups in both formations: (1) tear faults at high angles to structural trend, and (2) contraction faults. Tear faults and shear veins form single to conjugate sets that have accommodated wrench shear, small-scale block rotation, and minor tangential extension. Tear faults and associated veins formed over a protracted history: early faults have slip lineations subparallel to tilted bedding, and later faults have subhorizontal lineations. Most contraction faults are at low angles to bedding and formed early in the deformation history. Some contraction faults, however, cut fold limbs and formed during later fold tightening. Slip lineations on early contraction faults are at high angles to structural trend, whereas slip lineations on later faults have more east-west trends.

Minor folds in well-bedded intervals have hinge lines subparallel to structural trend. Fold wavelength is related to bed thickness, reflecting buckling during early LPS. Minor cross folds of bedding and cleavage with hinge lines at high angles to structural trend are locally developed in structurally complex settings near the salient ends and oblique ramps.

In summary, mesoscopic structures display kinematically consistent patterns in both the Twin Creek and Ankareh Formations (Fig. 7). Cleavage, high-angle fracture sets, contraction faults, and minor folds record widespread LPS. Cross-strike veins and fractures reflect minor tangential extension. Tear faults and en echelon vein arrays record wrench shear and local block rotation. Cleavage refraction records minor layer-parallel shear, and rare bed-parallel veins reflect minor extension down the dip of cleavage.

Timing Relations of Mesoscopic Structures

Structural relations around large-scale folds constrain timing relations of internal strain. Cleavage in both the Ankareh and Twin Creek Formations is fanned around most large-scale folds, remaining subperpendicular to bedding in fold limbs and hinge zones (Fig. 8). These relations indicate that cleavage formed during early LPS and was subsequently tilted along with bedding during large-scale folding and thrusting. Bed-parallel minor faults related to flexural slip, shear veins along cleavage seams in steep limbs, breccia zones between dip domains, and rare secondary cleavage record

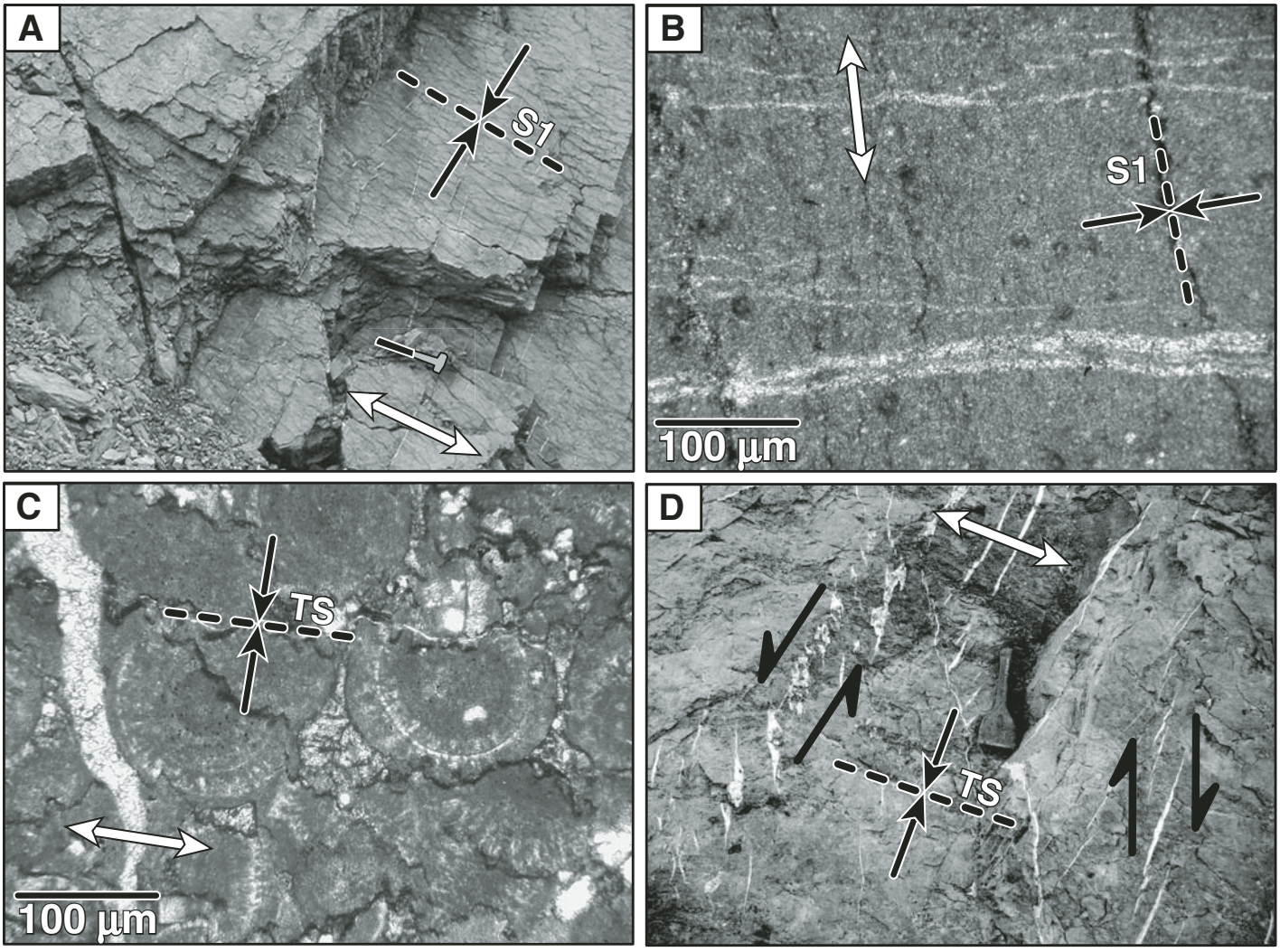

Figure 5. Structural style of the Jurassic Twin Creek Formation. (A) Outcrop along bedding planes showing spaced cleavage and veins in micritic limestone. Cleavage (S1) is defined by close-spaced partings at high angles to bedding and is interpreted to record early layer-parallel shortening directions (black arrows). Thin cross-strike veins record minor extension (white arrows) parallel to structural trend. Hammer for scale. (B) Photomicrograph of cleavage (S1) defined by spaced seams of dark material enriched in clays and depleted in calcite, which bound less deformed microlithons of micritic limestone. Seams both dissolve and are crosscut by calcite-filled veins. The amount of shortening (black arrows) can be estimated from seam widths. The amount of extension (white arrows) can be estimated from vein widths. (C) Photomicrograph of tectonic stylolites (TS) dissolving ooids. The amount of shortening (black arrows) can be estimated by amplitudes of stylolites and reconstructing original shapes of partly dissolved ooids. (D) Outcrop of bed-parallel surface with en echelon veins in zones at high angles to local fold axis and tectonic stylolites (TS). Chisel for scale.

internal strain during folding. Cross-strike veins and fractures, due to their geometric arrangement at high angles to fold axes, display limited changes in orientation during folding, making it difficult to determine timing relations based only on orientation. Crosscutting relationships, along with varying rakes of fiber lineations on shear veins, however, indicate that veins developed over a protracted history. Structural relations record an overall transition from more homogeneous strain, with development of cleavage and small-scale folds early in the deformation history, to more discrete deformation during large-scale folding and thrusting.

Textural relations preserved within clasts found in synorogenic conglomerates derived from uplift and erosion of the Crawford, Absaroka, and Hogsback systems further constrain timing relations. Cleavage seams preserved within clasts of Twin Creek limestone do not continue into conglomerate matrix and have random orientations, confirming that LPS occurred early in the deformation history of each thrust system, prior to erosion of clasts and conglomerate deposition (Mitra et al., 1984).

Orientation Analysis of Mesoscopic Structure

Orientations of bedding, cleavage, veins, and fracture sets were statistically analyzed for sites in the Twin Creek and Ankareh Formations (GSA Data Repository Tables DR1 and DR2[1]). At each site, 5–15 measurements were made

[1]GSA Data Repository item 2009097, tables listing mesoscopic structural and strain data, is available at http://www.geosociety.org/pubs/ft2009.htm or by request to editing@geosociety.org.

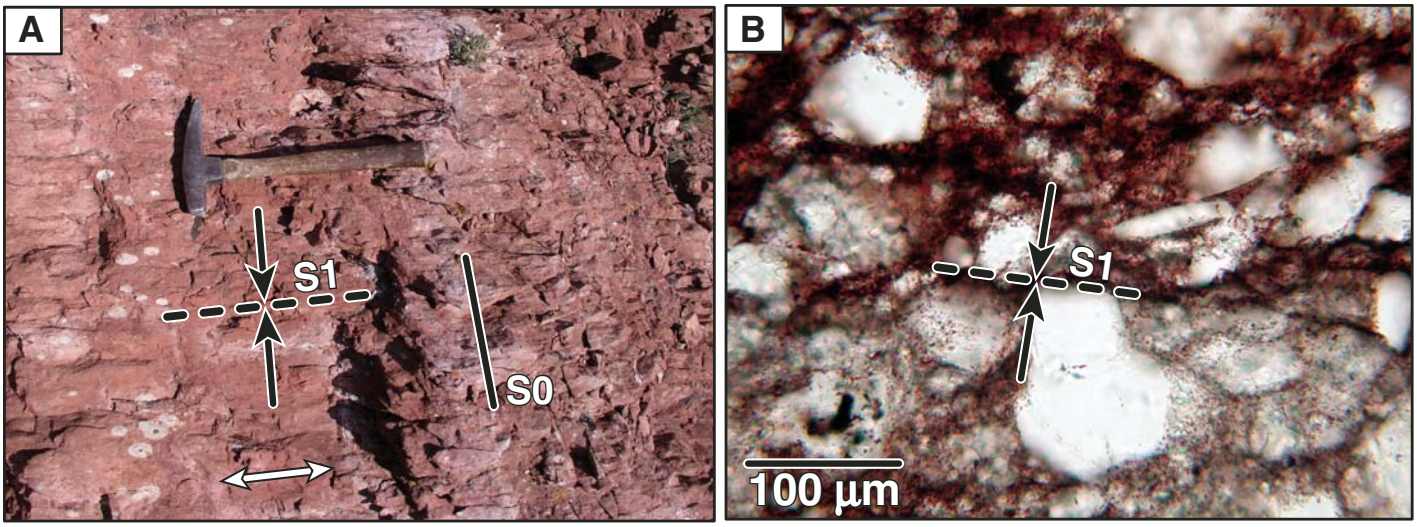

Figure 6. Structural style of the Triassic Ankareh Formation. (A) Outcrop showing spaced cleavage (S1) at high angles to bedding (S0) in calcareous mudstone. Cleavage is defined by partings at high angles to bedding and is interpreted to record layer-parallel shortening (LPS; black arrows). Reduction spots are elongate parallel to cleavage and provide a measure of finite strain, including a component of extension down the dip of cleavage (white arrows). Hammer for scale. (B) Photomicrograph of cleavage (S1) defined by discontinuous seams enriched in clay and hematite (black arrows). Seams were formed mostly by dissolution of calcite and quartz.

of each mesoscopic structure set. Fracture sets were defined based on persistence and consistent orientation. Fractures were not statistically analyzed for sites where limited outcrop size prevented identification of systematic sets. Poles to bedding and mesoscopic structures were plotted on stereograms, and mean orientations and α_{95} confidence cones were calculated using the orientation tensor method of Hext (1963).

Due to the complex deformation history in the salient, care was taken to restore tilted mesoscopic structures to their initial orientations. Directions of early LPS (based on orientations of cleavage and high-angle fracture sets) were estimated by restoring bedding to horizontal, using successive rotations determined from structural relations (Fig. 9). Most sites were located along limbs of horizontal folds or dip panels above frontal thrust ramps, and a single rotation about bed strike was used for restoration. For sites located along plunging folds, plunge was first removed, followed by rotation about the partly restored bedding strike. For sites located over oblique ramps, a single rotation about bed strike was used, although rotation histories may have been more complex. Some sites near the salient ends experienced additional tilting along margins of Laramide foreland uplifts and in footwalls of Neogene normal faults. Extension directions (based on orientations of cross-strike vein and fracture sets) were estimated by restoring bedding to horizontal. Although some veins likely formed during large-scale folding, partial unfolding paths did not significantly change estimated extension directions.

LPS directions estimated from cleavage and tectonic stylolites in the Twin Creek Formation are at high angles to structural trend and define a radial pattern around the salient (Fig. 10A). Extension directions estimated from cross-strike veins are subparallel to structural trend and define a tangential pattern (Fig. 10B). In detail, LPS and extension directions display minor (~10°) variations between nearby sites, partly reflecting local noise from small-scale, nonsystematic block rotations and stress-strain refraction. Patterns are more complex along oblique thrust ramps and near the salient ends where frontal thrusts interacted with foreland uplifts. Most veins are subperpendicular to structural trend, but veins are slightly oblique to trend at some sites (e.g., site TC51 in Fig. 9), reflecting rotation in en echelon arrays with a dominant sense of wrench shear.

LPS directions estimated from cleavage and high-angle fracture sets in the Ankareh Formation define an almost identical radial pattern (Fig. 11A). Extension directions define a corresponding tangential pattern (Fig. 11B). LPS and extension directions also display minor (~10°) variations between nearby sites due to local noise, and more complex patterns occur near oblique ramps and the salient ends. The similarity of patterns in the Twin Creek and Ankareh Formations, combined with reconnaissance studies of the Lower Triassic Thaynes Formation and the Cretaceous Gannett Group, indicates that LPS and extension directions are consistent through the stratigraphic section, although structural style varies with lithology.

Finite Strain Analysis

Twin Creek Formation

Finite strain in the Twin Creek Formation was estimated from: (1) spacing and widths of cleavage seams in micritic limestone; (2) amplitudes of tectonic stylolites in oolitic limestone; and (3) shapes of *Pentacrinus* ossicles in bioclastic limestone. Strain accumulated from multiple deformation mechanisms; mass transfer was dominant for cleavage seams and tectonic stylolites, and crystal plasticity (twinning and dislocation glide) was dominant in bioclastic limestone.

Shortening, S, in micritic limestone was calculated using a mass balance relation for dissolution of calcite within cleavage seams:

$$S = [c - (c/F)]/[m + (c/F)],$$

where c is the total width of cleavage seams, m is the total width of microlithons, and F is the volume fraction of insoluble material in the protolith (taken to be the same as in the microlithons). Note, shortening will be slightly underestimated if calcite has been removed from the microlithons by incipient dissolution and overestimated if some calcite remains in the seams. Spacing and amplitudes of tectonic stylolites provided a complementary measure of shortening by dissolution in oolitic limestone with micritic matrix; oolitic grainstones with sparry cement were deformed mostly by plastic twinning and contraction faulting.

Shapes of *Pentacrinus* ossicles were used to estimate bed-parallel strain in bioclastic lime-

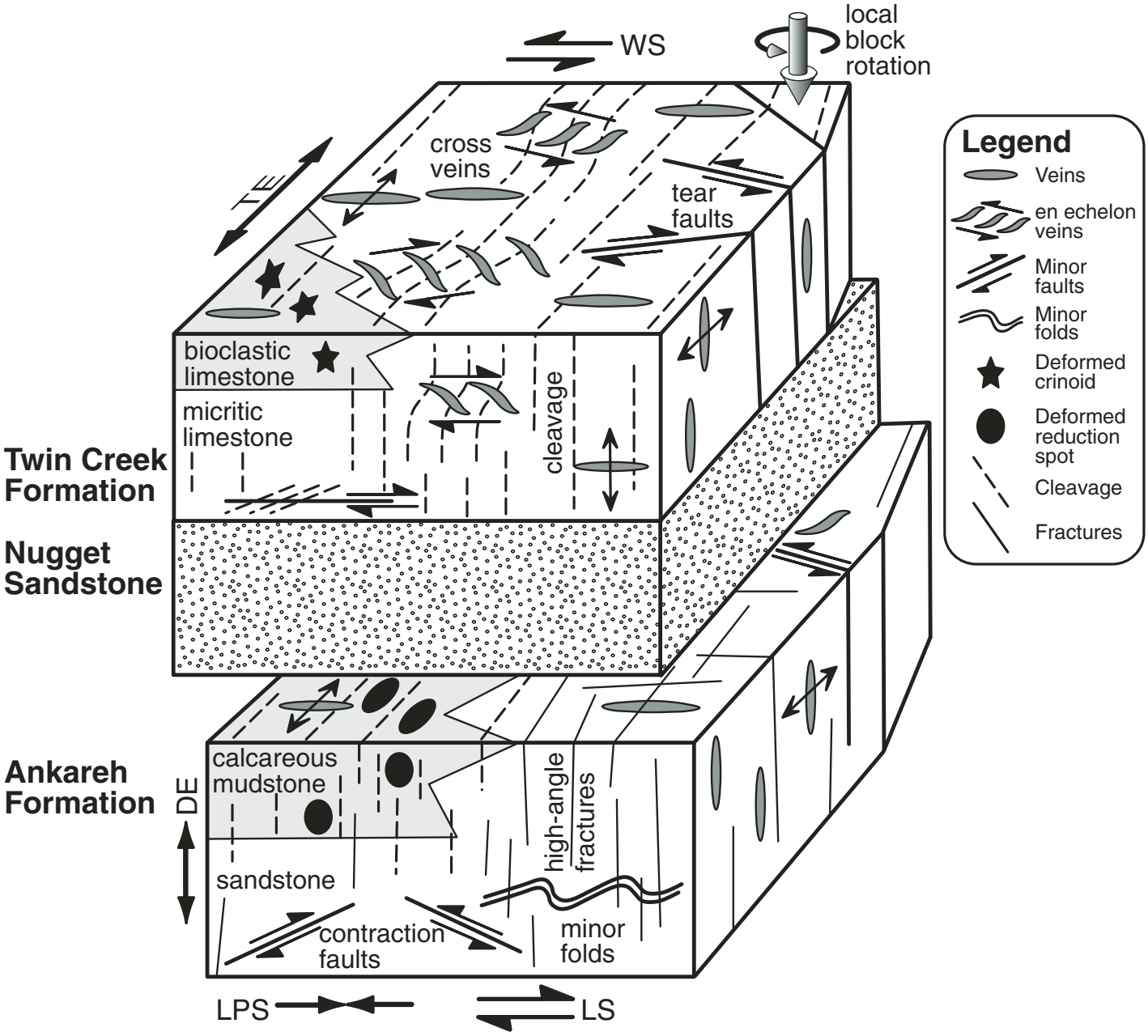

Figure 7. Block diagram illustrates typical relations of mesoscopic structures in the Twin Creek and Ankareh Formations, including cleavage (dashed lines), veins (gray filled), fractures (thin lines), and minor faults (thick lines). Cleavage is subperpendicular to bedding and formed during early layer-parallel shortening (LPS), with local refraction related to layer-parallel shear (LS). High-angle fractures, related to unloading following LPS, are also subperpendicular to bedding. Most veins are perpendicular to local fold axes and record tangential extension (TE). Some veins are grouped in en echelon arrays, which, along with tear faults, accommodated wrench shear (WS) and small-scale block rotations. Rare bed-parallel veins record minor extension down cleavage dip (DE). Minor folds and contraction faults accommodated minor shortening. Deformed fossils and reduction spots record principal shortening perpendicular to cleavage.

stone (Fig. 12). Undeformed crinoids have initial pentagonal symmetry, such that strain can be calculated using final arm lengths and angles. Where crinoids were present in sufficient numbers, an average strain ellipse was calculated using shapes of 10–30 ossicles. Based on structural relations, bedding approximated a principal strain plane, such that crinoid shapes recorded the ratio of LPS to tangential extension.

Widths of cleavage seams in micritic limestone and amplitudes of tectonic stylolites in oolitic limestone record 10%–30% shortening in areas with moderate to strong cleavage, 5%–10% shortening in areas with weak cleavage, and <5% shortening in areas where cleavage is absent (Fig. 13). Shortening varies locally due to heterogeneous pressure solution. Analysis of multiple samples from the Thomas Fork area (location

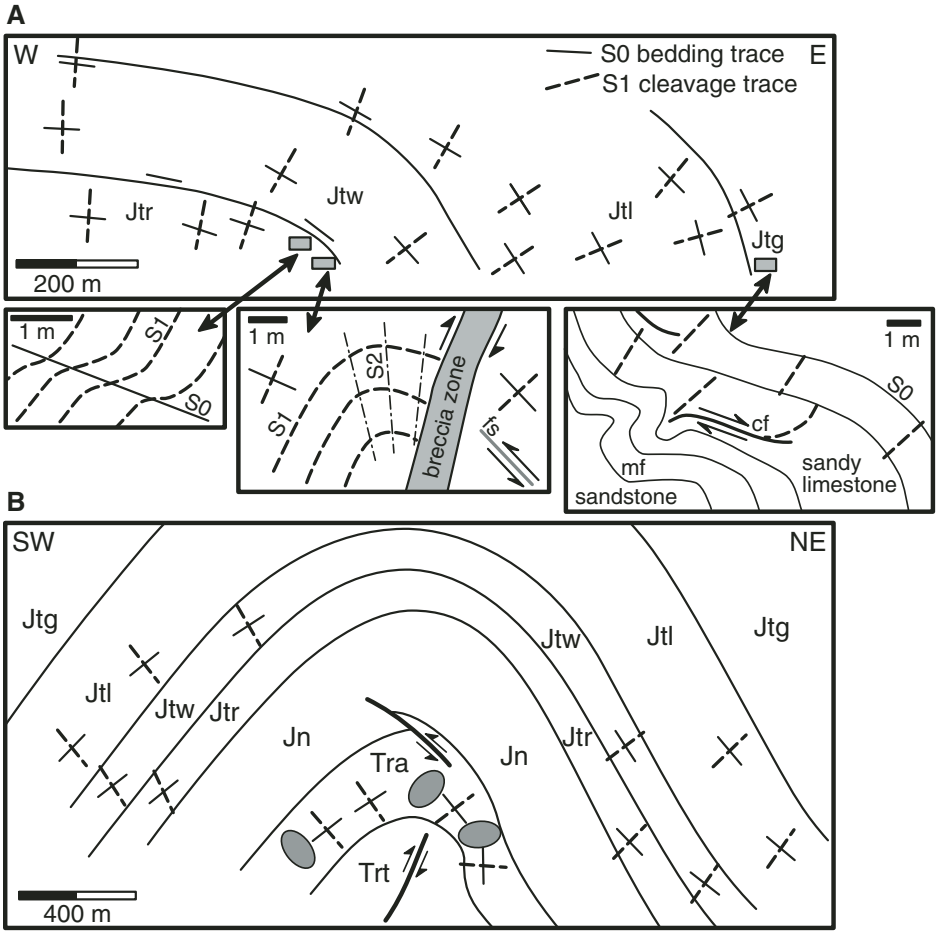

Figure 8. (A) Down-plunge projection of anticline in Thomas Fork area (location TF in Fig. 3A). Cleavage (dashed lines) is subperpendicular to bedding (thin lines) in both the fold crest and limbs, indicating that cleavage formed during early layer-parallel shortening (LPS) and was then rotated during large-scale folding and thrusting. Field sketches show from left to right: cleavage refraction related to early top-to-E shear along weak layers; flexural slip along bed-parallel surfaces (fs) and breccia zone with refolded cleavage and weak second cleavage (S2); and minor folds (mf) and contraction faults (cf) in well-bedded sandy limestone. Units are: Jtr—Rich to Gypsum Springs Members; Jtw—Watton Canyon and Boundary Ridge Members; Jtl—Leeds Creek Member; and Jtg—Giraffe Creek Member of the Twin Creek Formation. (B) Down-plunge projection of Big Elk anticline (location BE in Fig. 3A) illustrating similar structural relations in Twin Creek and Ankareh Formations. Cleavage (dashed lines) is strongly fanned about the fold. Strain ellipses, estimated from shapes of reduction spots in the Ankareh Formation, are also fanned about the fold and record early LPS. Additional units: Trt—Triassic Thaynes Formation, Tra—Ankareh Formation; Jn—Jurassic Nugget Formation.

TF, Fig. 13) yielded shortening estimates of 11% to 28%, with a mean of 18%. Widths of most cross-strike veins were 10^{-3}–10^{-2} m (with a few veins up to ~0.1 m wide), and typical spacings were 0.1–0.3 m, recording 1%–5% tangential extension at most sites. En echelon vein arrays and tear faults accommodated minor additional shear and tangential extension. Bed-parallel veins were less abundant and reflect <5% extension down cleavage dip.

Bed-parallel strain ellipses estimated from crinoids display systematic variations around the salient. Shortening directions define a radial pattern, and stretching directions define a corresponding tangential pattern (Fig. 13). Bed-parallel strain ratios range mostly from 1.15 to 1.3 in the Crawford system, whereas ratios in central parts of the Hogsback system are less than 1.05. Overall, cleavage intensity, shortening estimated from seam widths and stylolite amplitudes, and strain ratios calculated from crinoids increase westward and toward the salient ends.

Ankareh Formation

Finite strain in the Ankareh Formation was estimated using shapes of reduction spots in calcareous mudstone to fine-grained sandstone (Fig. 14A). Reduction spots are locally offset across fractures and veins, but they typically do not show additional growth along these features, indicating that spots grew mostly prior to deformation and can be used to estimate strain. Where reduction spots were present in sufficient numbers, shapes of 15–30 spots were measured on each of three approximately perpendicular surfaces (including a bed-parallel surface). Two-dimensional fabric ellipses were calculated with the Rf-ϕ method (Fig. 14B), using the tensor approach of Shimamoto and Ikeda (1976). Uncertainties in ellipse ratios and directions were evaluated using bootstrap statistics (Fig. 14C). For moderately strained sections, ellipse ratios and directions had typical 2σ (95%) uncertainties of about ±0.1 and ±8°. Principal directions and axial ratios of three-dimensional fabric ellipsoids were calculated from two-dimensional data using the method of Owens (1984). Confidence intervals for principal directions and ratios were evaluated using Monte Carlo simulations (Fig. 14D), following Yonkee (2005).

Principal directions and ratios of fabric ellipsoids are illustrated in Figure 15 (see GSA Data Repository Table DR3 for details [see footnote 1]). The final ellipsoid reflects both a primary sedimentary fabric and tectonic strain. Very low-strain sites have oblate fabric ellipsoids with approximately circular sections along bedding surfaces (inset in Fig. 14A) and axial ratios of $R_{YZ} \approx 1.1$ on surfaces perpendicular to bedding (where $X \geq Y \geq Z$ are the principal axes of the fabric ellipsoid; Fig. 15A). These relations are consistent with ~10% sedimentary compaction and Z (shortening) directions initially perpendicular to bedding (stage 1 in Fig. 16). This primary fabric was modified by increasing components of LPS and tangential extension during progressive deformation. Section ellipses on trend-parallel planes become slightly more elongate as tangential extension increases. Ellipses on trend-perpendicular (profile) planes display more complex patterns, first becoming more circular as LPS increases to 10% (stage 2), and then becoming more elliptical with Z directions switching to bed-parallel as LPS increases (stage 3 in Fig. 16). Low-strain sites have prolate ellipsoids with R_{XY} approaching 1.2 as LPS increases to 10%, poorly defined Z directions, and X directions parallel to structural trend, which reflect mixed sedimentary and tectonic

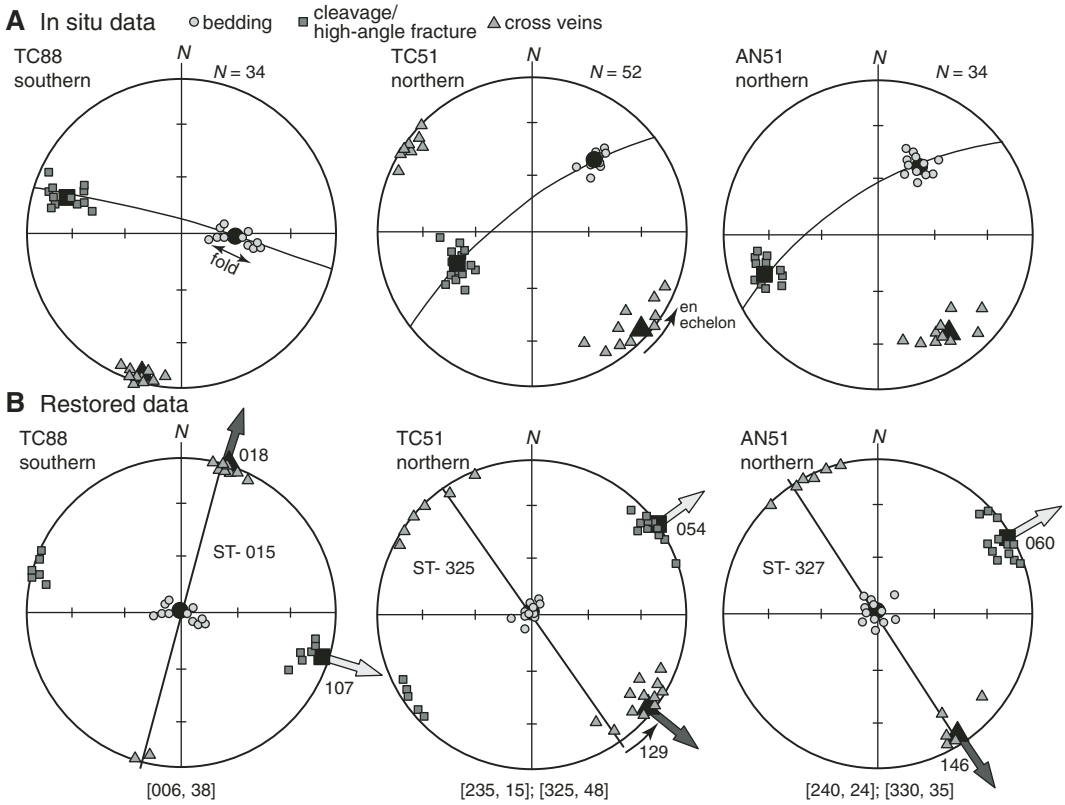

Figure 9. Equal-area stereograms illustrating typical geometric relations of bedding and mesoscopic structures for study sites. Poles to bedding are plotted as circles (mean given by large circle), poles to cleavage are plotted as squares (mean given by large square), and poles to veins are plotted as triangles (mean given by large triangle). (A) In situ stereograms for Twin Creek site TC88 from southern part of the salient, Twin Creek site TC51 from northern part of the salient, and nearby Ankareh site AN51. Cleavage poles are subperpendicular to bedding poles, which show limited folding at some sites. Most vein poles are parallel to the local fold axis but are rotated in en echelon arrays. Orientations of cleavage and veins are different between southern and northern parts of the salient, but they are similar for nearby sites in the Twin Creek and Ankareh Formations. (B) Restored stereograms for same sites as in A. Rotations (trend of axis, angular degrees) used to restore bedding to horizontal are given in brackets. Site TC88 was restored by a single rotation about bed strike; sites TC51 and AN51 also included removal of fold plunge. Initial layer-parallel shortening (LPS) directions estimated from restored cleavage (indicated by gray arrows) range from ESE for the southern site to ENE for the northern sites. Extension directions estimated from veins (indicated by black arrows) range from NNE in the southern site to NNW in the northern sites, subparallel to the large-scale structural trend (ST) near each site (indicated by solid line).

fabrics (Fig. 15). Medium- to high-strain sites typically have *Z* directions parallel to bedding and increasing R_{YZ} as LPS increases, reflecting a dominant tectonic fabric. A decrease in R_{XY} for some high-strain sites indicates minor extension down cleavage dip (Fig. 15A). A few sites from tight folds have *Z* directions and cleavage at acute angles to bedding, reflecting additional strain during folding.

At medium- to high-strain sites, tectonic shortening (*Z*) directions are subparallel to cleavage poles. Angular residuals between shortening directions and cleavage poles have a small standard deviation of $\sigma_r = 7°$ related to measurement uncertainties. In low-strain areas, tectonic shortening directions (which are perpendicular to *X* fabric directions) are roughly parallel to poles of high-angle fracture sets, but they have slightly greater $\sigma_r = 12°$. Thus, poles to cleavage and high-angle fracture sets provide reasonable proxies for shortening directions.

Bed-parallel strain ellipses record the ratio of LPS to tangential extension (TE) (where $R \approx [1 + TE]/[1 - LPS]$) and display systematic regional variations. LPS directions define a radial pattern, and extension directions define a corresponding tangential pattern around the salient (Fig. 17). Bed-parallel strain ratios range from 1.3 to 1.6 in the Crawford system, whereas ratios are less than 1.1 in central parts of the Hogsback system; ratios also increase overall toward the salient ends.

Comparison of Strain Estimates

Orientations and magnitudes of finite strain are broadly similar for the Ankareh and Twin Creek Formations. In detail, bed-parallel strain ratios for reduction spots in Ankareh red beds are slightly greater than ratios for crinoids in Twin Creek limestones. This may reflect an overestimate of strain in red beds due to a component of diffusion-controlled growth of spots parallel to cleavage fabrics (Nakamura and Borradaile, 2001), or an underestimate of strain from crinoids in bioclastic limestone that also

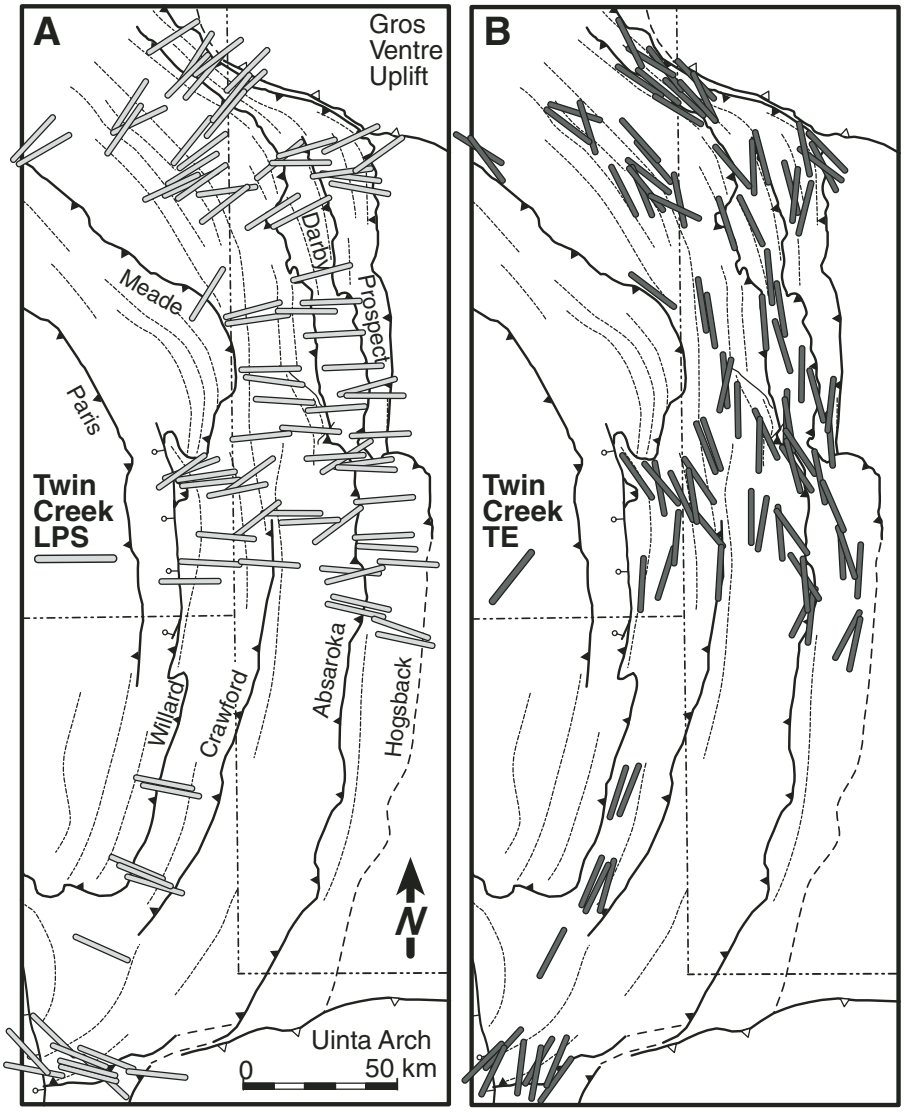

Figure 10. Restored deformation fabric directions for Twin Creek sites. (A) Layer-parallel shortening (LPS) directions estimated from cleavage and tectonic stylolites define an overall radial pattern. (B) Extension directions estimated from cross-strike veins define a tangential extension (TE) pattern.

shortened by contraction faulting in addition to plastic deformation recorded by fossils. Differences in ratios between red beds and limestones, however, are small and closely bracket strain estimates.

Strain compatibility requires magnitudes and directions of LPS and tangential extension to be similar between different layers, unless there is simple shear or a detachment between layers. Volume loss, however, may vary between layers and must be known for accurate restorations of initial stratigraphic thicknesses and sedimentary prism taper. Cleavage seam widths in micritic limestone of the Twin Creek Formation record 10%–30% LPS by mass transfer deformation in medium- to high-strain areas, whereas vein widths record ~5% tangential extension and minor extension down cleavage dip (DE), consistent with 5%–20% volume loss. Plastic deformation of crinoids in bioclastic limestone was likely isovolumetric. Bed-parallel ratios of $R \approx [1 + \mathrm{TE}]/[1 - \mathrm{LPS}] \approx 1.15–1.3$ in medium- to high-strain areas are consistent with 10%–20% LPS, ~5% tangential extension, and 5%–15% downdip extension (DE). Reduction spots in Ankareh red beds have bed-perpendicular ratios of $R_{XY} \approx [1 + \mathrm{TE}]/[0.9 + \mathrm{DE}] \approx 1.1–1.2$, and $R_{YZ} \approx [0.9 + \mathrm{DE}]/[1 - \mathrm{LPS}] \approx 1.2–1.4$ in medium- to high-strain areas, consistent with 20%–30% LPS, ~5% tangential extension, minor DE, and 10% initial sedimentary compaction. In summary, cleavage seam widths, crinoid shapes, and reduction spot fabrics indicate 10%–30% LPS in medium- to high-strain areas, 5%–10% LPS in low-strain areas, and <5% LPS in very low-strain areas, along with ~5% tangential extension and variable volume loss.

Relations between Deformation Fabric Directions and Regional Structural Trend

Correlations between deformation fabric directions (estimated from cleavage, high-angle fractures, cross-strike veins, crinoids, and reduction spots) and map-view curvature were quantitatively evaluated using a strike test. For a strike test, LPS and tangential extension directions relative to a reference direction of E-W/N-S were plotted against structural trend relative to a reference trend of N-S. Data were fit to a linear model using a weighted least-squares method that incorporated measurement uncertainty and structural noise (for a brief description of methods, see Appendix A of Weil et al., 2009). The calculated strike-test slope gives the fraction of variation in fabric direction correlated to change in structural trend. Sites from overturned fold limbs, oblique ramps, and transfer zones had more complex histories and displayed outlier directions. Thus, results for filtered data sets that exclude these sites are presented first, followed by examples from complex structural settings.

Twin Creek Formation

The Twin Creek Formation had 118 sites (plus 14 subsites) located in uncomplicated (filtered) settings, 24 sites (plus 1 subsite) located in complex settings (overturned fold limbs, oblique ramps, and transfer zones), and two sites located in adjacent margins of foreland uplifts. Most filtered sites displayed cleavage or tectonic stylolites related to early LPS. A strike test of filtered LPS directions yielded a best-fit slope of 0.92 with a 2σ (95%) confidence interval of ±0.07, based on weighting factors that included local noise $\sigma_n = 8°$ (Fig. 18A). Most sites also displayed cross-strike veins related to extension, plus minor shear in en echelon arrays. A strike test for vein orientations yielded a best-fit slope of 0.99 with a 2σ (95%) confidence interval of ±0.07 (Fig. 18B). The slightly higher slope partly reflects minor rotation of veins in en echelon arrays, that tend to have more sinistral shear in the northern part of the salient and more dextral shear in the southern part.

Ankareh Formation

The Ankareh Formation had 127 sites from uncomplicated (filtered) settings, 25 sites from complex settings (overturned fold limbs, oblique ramps, and transfer zones), and two sites from

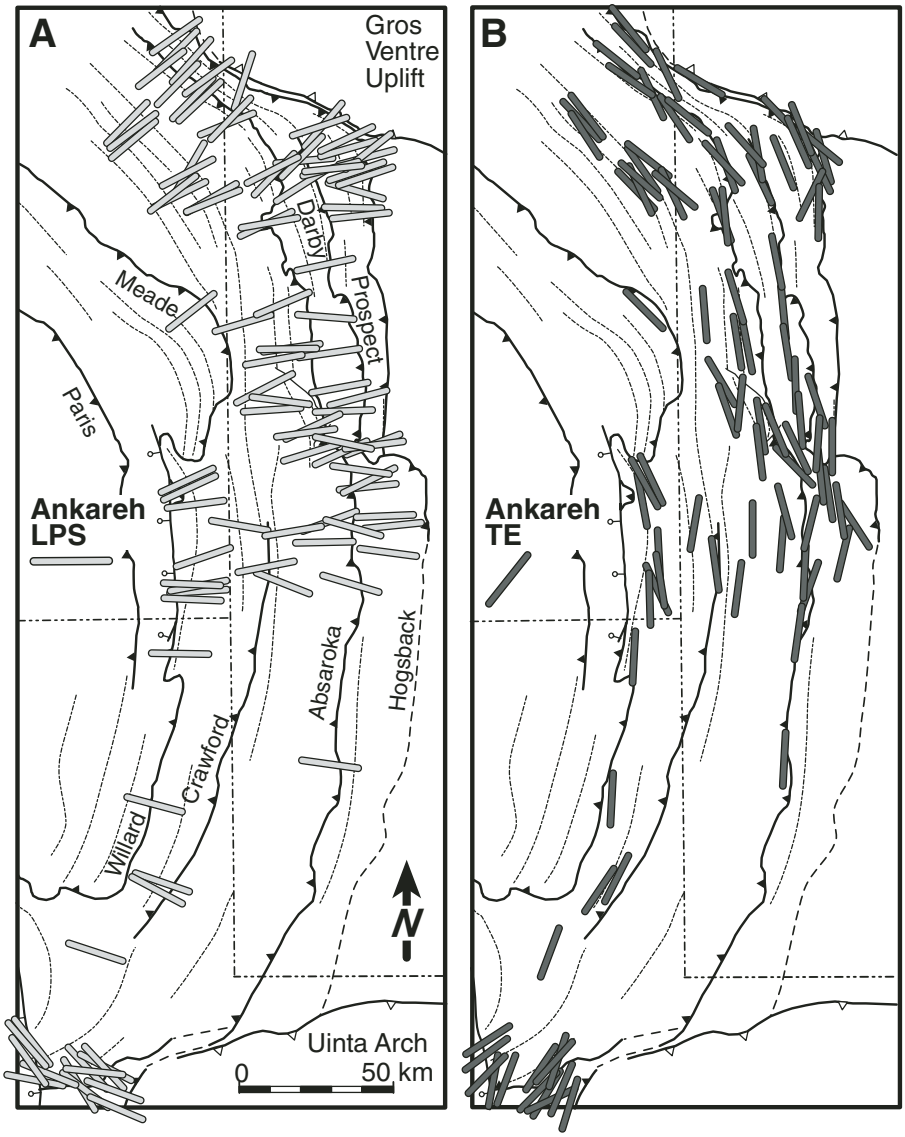

Figure 11. Restored deformation fabric directions for Ankareh sites. (A) Layer-parallel shortening (LPS) directions estimated from cleavage and high-angle fracture sets define an overall radial pattern, similar to relations in the Twin Creek Formation. (B) Extension directions estimated from cross-strike fractures and veins define a tangential extension (TE) pattern.

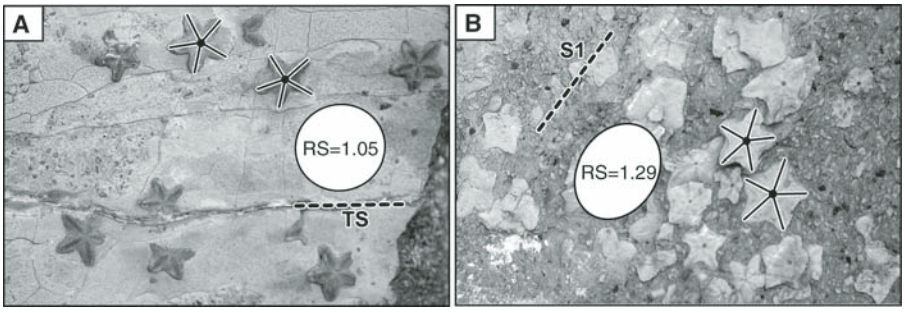

Figure 12. Examples of crinoid ossicles along bed-parallel surfaces in the Twin Creek Formation used to estimate strain. (A) Crinoids at very low-strain site with widely spaced tectonic stylolites (TS) have approximate pentagonal symmetry. (B) Deformed crinoids at a higher-strain site with cleavage (S1) yield a strain ratio (RS) of 1.29.

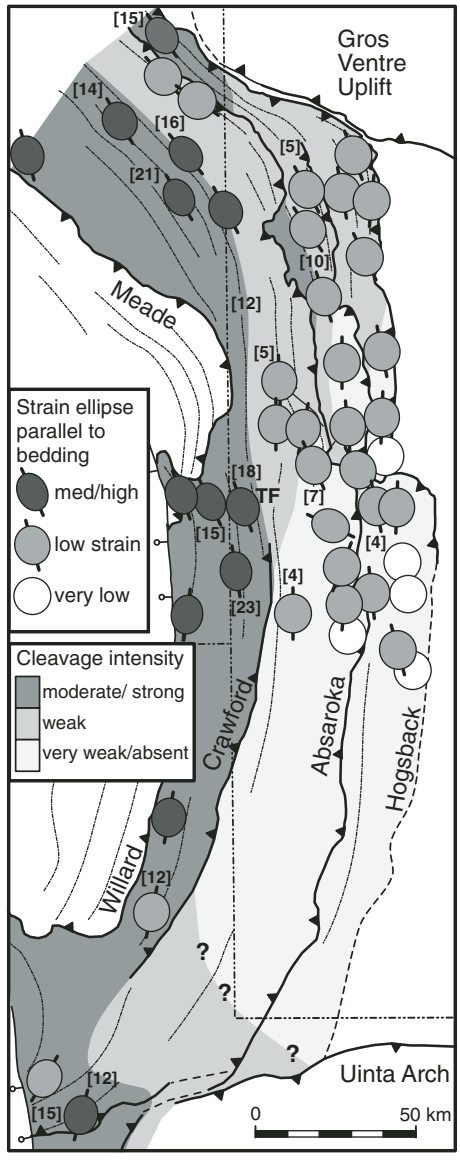

Figure 13. Map of bed-parallel strain ellipses estimated from crinoid ossicle (which approximately record the ratio of layer-parallel shortening [LPS] to tangential extension), LPS estimated from cleavage seam widths and stylolite amplitudes (% shortening listed in brackets), and cleavage intensity for micritic limestone in the Twin Creek Formation. Strain ratios, LPS estimates, and cleavage intensity increase overall westward into the Crawford system and toward the salient ends. TF—Thomas Fork area.

adjacent margins of foreland uplifts. Of the filtered sites, LPS directions were estimated from cleavage orientations at 36 sites and from high-angle fracture sets at 69 sites. Some sites had oblique fractures that did not form regionally consistent sets and were uncorrelated with structural trend. A strike test of filtered LPS directions estimated from cleavage yielded a best-fit slope of 0.88 ± 0.10 (2σ) (Fig. 19A), statistically identical to the slope of 0.89 ± 0.12 (2σ) calculated from principal strain directions for reduction spots (Fig. 19C). Directions estimated from high-angle fractures yielded a slightly higher slope of 0.95 ± 0.10 (2σ), which may partly record fracturing during large-scale folding. Most Ankareh sites displayed cross-strike veins and fracture sets related to extension, which yielded a best-fit slope of 0.96 ± 0.07 (2σ) (Fig. 19B).

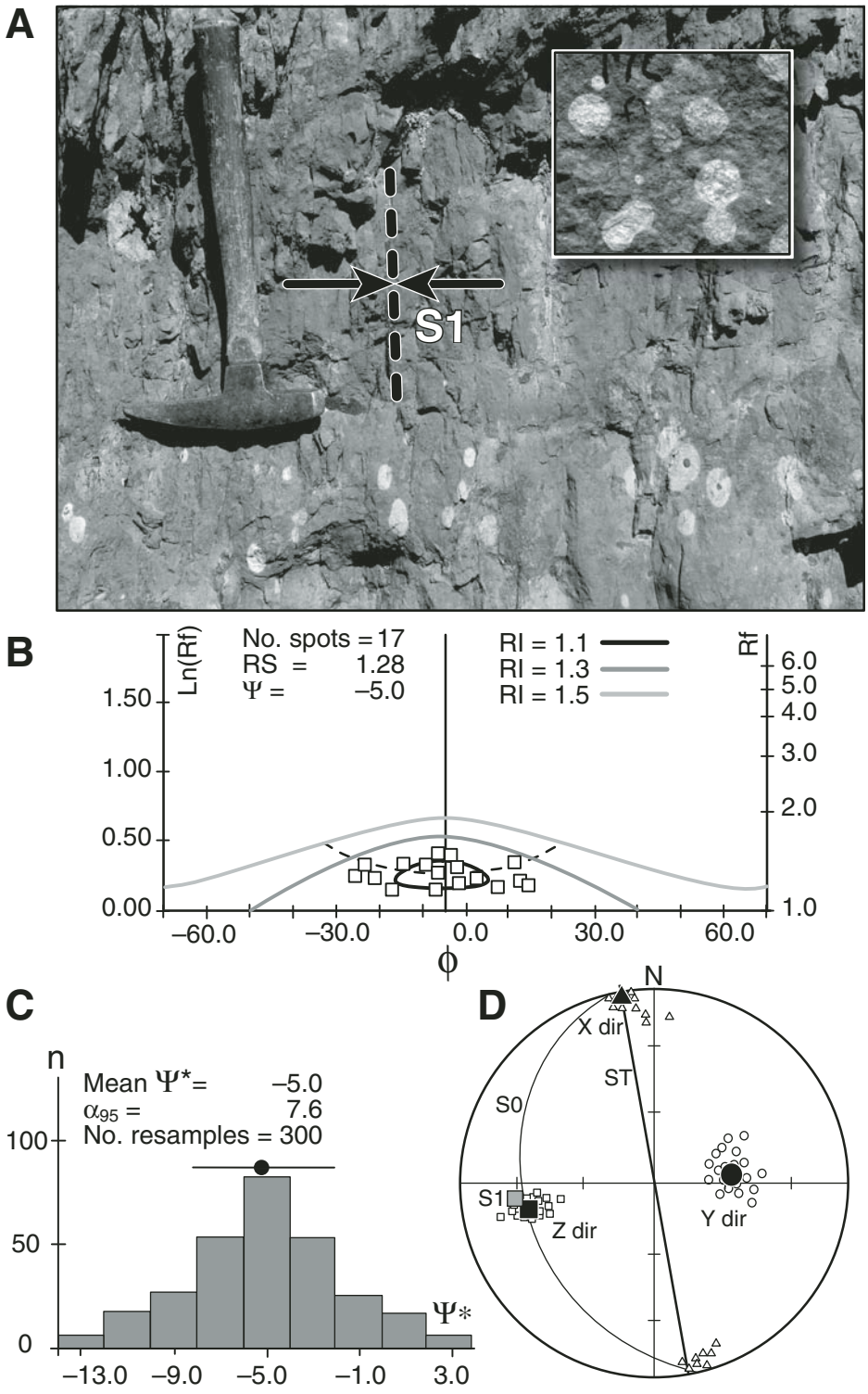

Figure 14. Methods of finite strain analysis for reduction spots in the Ankareh Formation. (A) Reduction spots have elliptical shapes subparallel to cleavage (S1) at more deformed sites. Inset shows circular spots along bedding from a relatively undeformed site in the foreland. (B) Example of two-dimensional finite strain data from site AN17. Rf-ϕ plot for reduction spots along bed-parallel surface has two-dimensional strain ratio RS = 1.28 and stretching direction Ψ = –5.0° calculated using tensor method. Curves shown for initial ratios RI = 1.1, 1.3, and 1.5 indicate reduction spots started close to circular. (C) Histogram of estimated stretching directions for bootstrap resamples (Ψ*) from bed-parallel plane, with mean of –5.0° and 95% confidence interval of ±7.6°. (D) Stereogram of best-fit three-dimensional strain directions calculated from data for three planes at site AN17 (with *X* > *Y* > *Z*; solid symbols are scaled to α_{95} of 6°). Example directions for 20 Monte Carlo simulations are shown by open symbols. *Z* direction is subparallel to cleavage (S1) pole and bedding (S0). *X* direction is subparallel to structural trend (ST).

In summary, strike tests yielded similar slopes for both formations. LPS directions estimated from cleavage and finite strain directions are about, but not precisely, perpendicular to structural trend. Strike tests were also performed for sites grouped into domains corresponding to the Crawford, Absaroka, and Hogsback systems to evaluate any differences in deformation fabric directions between thrust sheets emplaced at different times. Slopes were statistically indistinguishable between thrust systems, indicating that LPS orientation patterns remained consistent, even though LPS fabrics in various systems may have formed at different times.

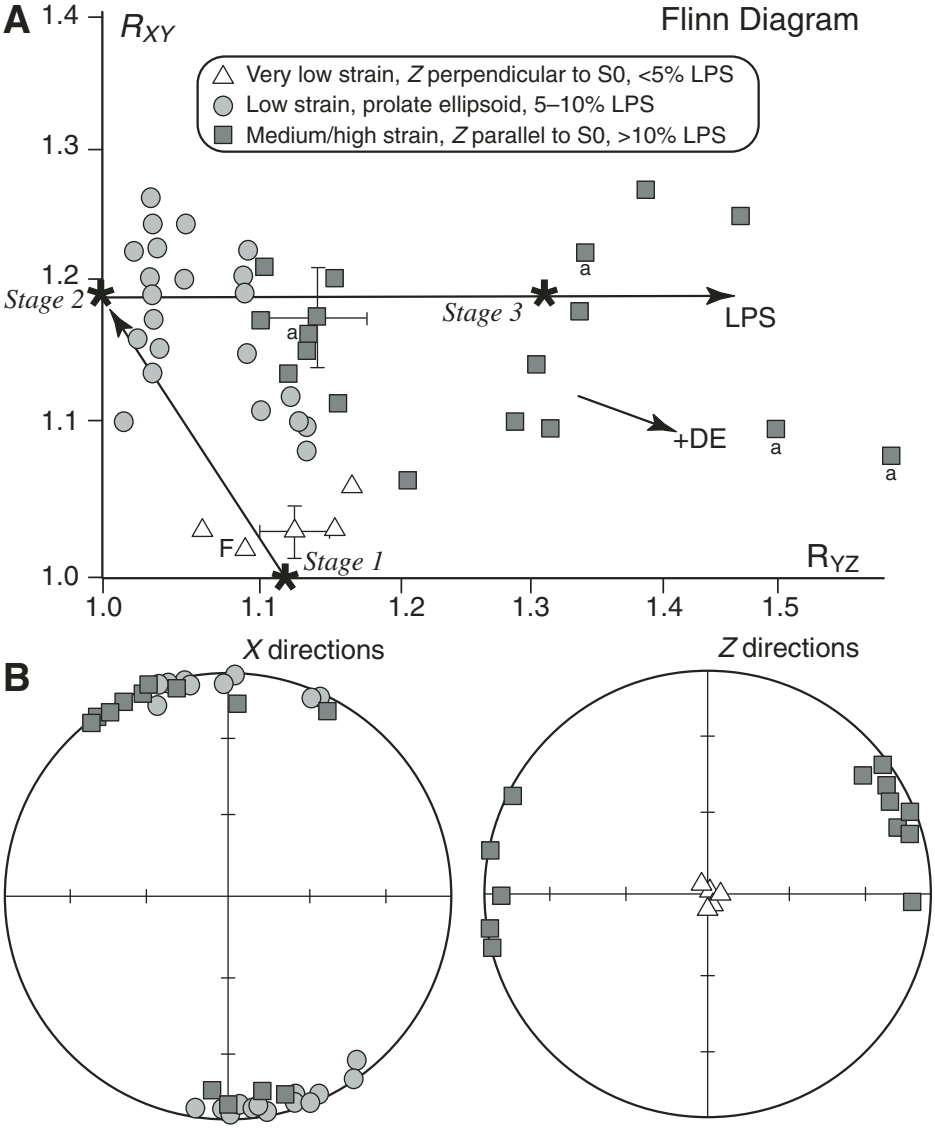

Figure 15. Results of three-dimensional strain analysis for reduction spots in the Ankareh Formation. (A) Flinn diagram of final fabric axial ratios; a—cleavage at acute angles to bedding. Very low-strain sites (triangles) have oblate shapes with $R_{YZ} \approx 1.1$; site F is from the foreland. Low-strain sites (circles) have prolate shapes with $R_{XY} \approx 1.1–1.2$, reflecting ~5%–10% layer-parallel shortening (LPS). Moderate- to high-strain sites (squares) display increasing R_{YZ} as LPS increases. Minor extension down cleavage dip (DE) decreases R_{XY}. Path and ratios are indicated for idealized fabric stages shown in Figure 16. (B) Principal fabric directions for bedding restored to horizontal. *X* directions are gently plunging and subparallel to structural trend. *X* directions are poorly defined and not plotted for very low-strain sites. *Z* directions are subparallel to bedding for medium- to high-strain sites but are perpendicular to bedding for very low-strain sites in which bedding compaction is dominant. *Z* directions are not plotted for low-strain sites with prolate ellipsoids or sites with acute cleavage angles.

Structurally Complex Areas

Evaluation of local complications is important for understanding regional kinematic evolution. Here, we discuss complications along oblique ramps and from interaction with foreland uplifts near the salient ends, as exemplified by the Beaver Creek, Granite Creek, and Parleys Canyon areas (Fig. 20).

The Beaver Creek area, which was previously studied by Apotria (1995), exposes a moderately dipping (~30°–50°) panel of Triassic to Jurassic strata with a distinct bend in strike from a regional average of ~005° to locally ~320° (Fig. 20A). The change in strike coincides with a bend in the frontal trace of the Absaroka thrust and an oblique ramp in the South Fork thrust (a hanging-wall imbricate). Oblique structural trends in the area, along with orientations of LPS fabrics, may be interpreted as resulting from: (1) mostly horizontal-axis rotation of the hanging-wall panel about the strike of bedding; or (2) vertical-axis rotation superimposed on the regional structural trend. LPS fabrics restored using path 1 roughly match regional shortening directions found north and south of the bend, whereas fabrics restored using path 2 yield directions inconsistent with regional patterns (Fig. 20A). These results suggest that sampled sites experienced only minor (≤10°) vertical-axis rotation as they were tilted above the oblique ramp. Localized folds with westerly trending hinge lines may record partitioning of wrench shear and shortening near the oblique ramp (Apotria, 1995). Similar relations for sites near other moderately dipping oblique panels also suggest limited vertical-axis rotation, whereas sites near steep tear faults display significant changes in fabric directions. Initial LPS directions, however, may vary due to complex stress patterns near oblique ramps, making it difficult to quantify rotation unless paleomagnetic data are available (Weil et al., 2009).

The Granite Creek area lies near the northern part of the salient where frontal thrusts interacted with the Gros Ventre foreland uplift (Fig. 20B). Seismic and drill-hole data record the subsurface position of the Granite Creek thrust, which has a substantial northward increase in slip that matches a corresponding decrease in slip on the Darby thrust to the west (Hunter, 1988; Royse, 1993). The Granite Creek sheet was partly eroded and buried by Paleocene strata, followed by emplacement of the out-of-sequence Cliff Creek and Game Creek thrusts, synchronous with major foreland uplift (Hunter, 1988). Out-of-sequence thrusting was likely related to foreland buttressing. Early LPS directions in the Twin Creek and Ankareh Formations trend ENE in much of the area, but they trend ESE in the southern part of the area (site TC100, Fig. 20B),

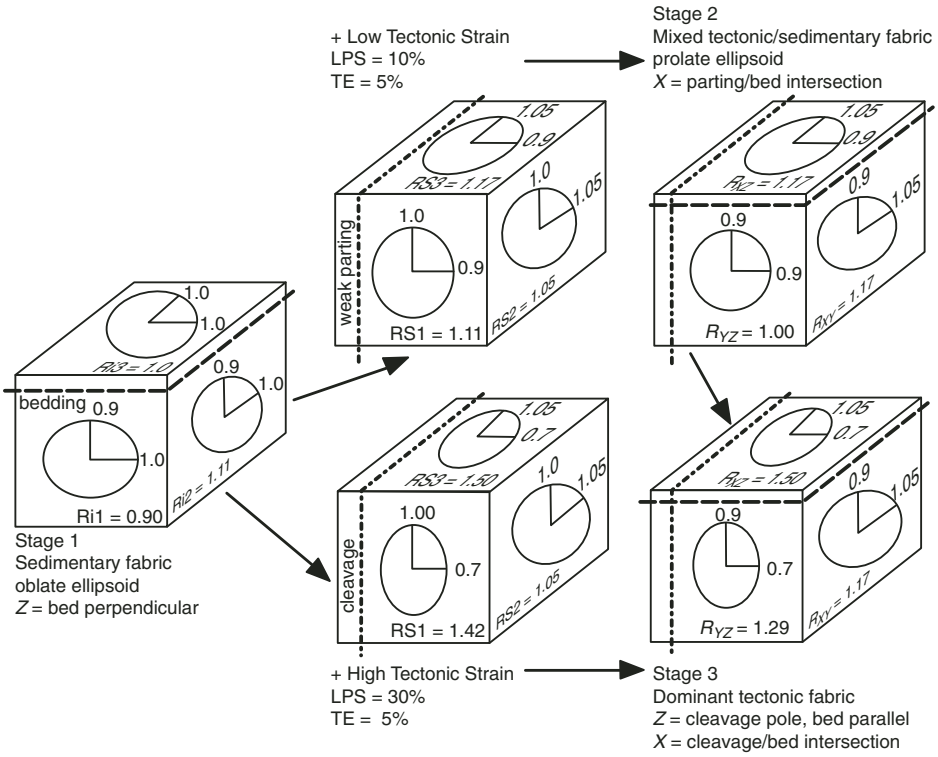

Figure 16. Model of reduction spot fabrics during progressive deformation. Stage 1 has a weak primary fabric parallel to bedding related to sedimentary compaction. Stage 2 superimposes a low tectonic strain (10% layer-parallel shortening [LPS] and 5% tangential extension [TE]) on the primary fabric to produce a prolate final ellipsoid with long axis parallel to the intersection of a weak parting and bedding. Stage 3 has a higher tectonic strain (30% LPS and 5% TE) that produces a final ellipsoid perpendicular to bedding and parallel to strong cleavage. The final fabric ellipsoid represents the product of the initial and tectonic strain ellipsoids, with ellipse ratios indicated on profile (1), tangential (2), and bed-parallel (3) faces.

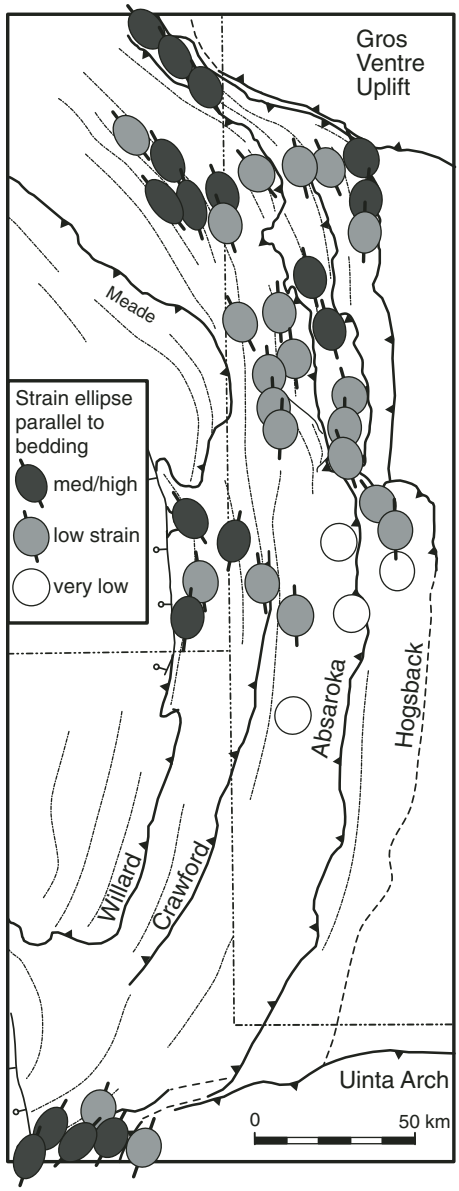

Figure 17. Map of bed-parallel strain ellipses for Ankareh Formation, which approximately record the ratio of layer-parallel shortening (LPS) to tangential extension (TE). Strain ellipses are about circular in central parts of the Hogsback system, but strain ratios increase westward into the Crawford system and toward the salient ends. Shortening directions (short axes of ellipses) define a radial pattern around the salient.

consistent with local clockwise rotation related to a northward increase in slip on the subsurface Granite Creek thrust. N to NNW structural trends were then superimposed on early LPS fabrics during slip on the out-of-sequence Cliff Creek thrust. Additional complications developed in the northern part of the area during impingement of the Gros Ventre uplift, including tear faults, cross folds (sites TC01 and TC02), and tilting near the WNW-trending Cache Creek reverse fault (site TC104, Fig. 20B). Restoration of cross folds and foreland tilting yields ENE directions for early LPS. Cross folds also accommodated local tangential shortening and minor vertical-axis rotation. A zone of concentrated deformation continues 30 km WNW into the Teton Pass area, where Triassic red beds underwent up to 60° counterclockwise rotation (Grubbs and Van der Voo, 1976), recording localized sinistral transpression along the front of the thrust wedge as it was being sheared and overridden by the growing foreland uplift. The more internal Absaroka and Crawford systems display gradual rather than abrupt counterclockwise changes in structural trend and LSP directions that appear related to regional stratigraphic changes, indicating that effects of foreland buttressing were confined to the leading edge of the thrust belt.

The Parleys Canyon area lies near the southern part of the salient where the Absaroka thrust system (including the Mount Raymond thrust) was tilted about the Uinta-Cottonwood Arch, providing an oblique-plunge view of the thrust system (Fig. 20C). The Uinta-Cottonwood Arch is a major E-W–trending foreland uplift that formed mostly during the latest Cretaceous to Eocene (Bradley and Bruhn, 1988). The arch projects beneath the Sevier thrust belt, separating the Wyoming salient to the north from the Charleston salient to the south (Paulsen and Marshak, 1997; Conder et al., 2003). The Uinta-Cottonwood Arch makes up the main Uinta Range to the east and projects westward beneath the Sevier thrust belt. The Mount Raymond thrust has a ramp-flat geometry, and was active during the Late Cretaceous (Bradley and Bruhn, 1988). A series of NNE-trending folds developed between a lower detachment in Permian shale and an upper detachment in Jurassic strata that merged eastward into the Mount Raymond thrust. The Ankareh

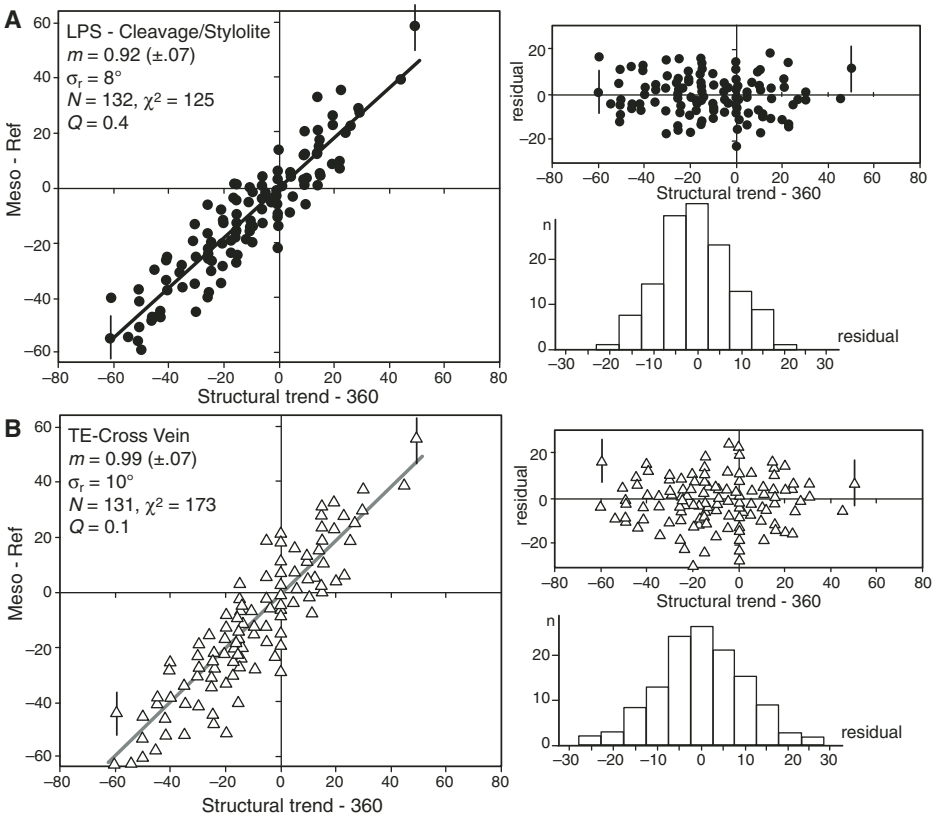

Figure 18. Strike-test results for deformation fabrics in the Twin Creek Formation. (A) Plot of filtered layer-parallel shortening (LPS) directions (relative to a reference 090°) estimated from cleavage and tectonic stylolites versus structural trend (relative to a reference 360°). Data show a strong correlation with a best-fit slope (*m*) of 0.92 and 2σ (95%) confidence interval of ±0.07. Standard deviation of residuals, σ_r, total weighted misfit, χ^2, number of sites, *N*, and goodness of fit, *Q*, are listed. Example 1σ error bars for individual site values are indicated, based on measurement uncertainty combined with structural noise of $\sigma_n = 8°$. Residuals are uncorrelated with trend and have a normal distribution. (B) Plot of extension directions (relative to a reference 360°) estimated from cross-strike veins versus structural trend. Data define a best-fit slope of 0.99 and 2σ (95%) confidence interval of ±0.07. Example 1σ error bars for individual site values are indicated. Larger residuals reflect additional rotation of veins in en echelon arrays.

and Twin Creek Formations display a dominant cleavage (S1) that formed during early LPS and was fanned about the detachment folds. A weak second cleavage (S2), which transects the detachment folds, developed during subsequent NNW tilting along the flank of the Uinta-Cottonwood Arch. Axial traces of the detachment folds (which have steeply dipping axial planes) retained overall NNE trends during tilting, whereas the trace of the gently dipping Mount Raymond thrust was strongly modified. Orientations of S1 cleavage, restored for tilting, indicate early LPS was to the ESE (e.g., sites TC80 and TC81, Fig. 20C). Fault-slip lineations, restored for tilting, also trend ESE but are oblique to current thrust traces (site RP, Fig. 20C). Structural relations thus record early ESE LPS and detachment folding, followed by ESE-directed slip on the Mount Raymond thrust, NNW tilting along the Uinta-Cottonwood Arch, and final Neogene tilting in the footwall of the Wasatch normal fault.

Regionally, the Absaroka system displays gradual clockwise changes in structural trend and LPS directions toward the southern end of the Wyoming salient, which appear related to regional stratigraphic thinning to the south. The current E-W–trending Mount Raymond trace thus mostly reflects tilting along the Uinta-Cottonwood Arch rather than abrupt clockwise rotation and wrench faulting, similar to conclusions reached by Paulsen and Marshak (1997). Early, minor uplift of the Uinta-Cottonwood Arch may have favored increased LPS toward the salient end. Interaction between the Hogsback thrust and Uinta-Cottonwood Arch to the east may have resulted in local dextral transpression, but relations are obscured by younger deposits (Bradley and Bruhn, 1988).

DISCUSSION

Summary of Strain Patterns and Comparison to Previous Studies

Mesoscopic structures and strain fabrics in the Jurassic Twin Creek and Triassic Ankareh Formations display systematic patterns around the Wyoming salient. Cleavage, tectonic stylolites, high-angle fractures, minor folds, and contraction faults accommodated LPS that largely preceded large-scale folding in each thrust system. Cross-strike veins and tear faults accommodated minor tangential extension and wrench shear over a protracted history. LPS directions define an overall radial pattern around the salient, and extension directions define a tangential pattern. Slip lineations on minor faults and shear veins vary from perpendicular to structural trend to roughly E-W. Analysis of cleavage seam and vein widths, crinoid ossicles, and reduction spots provides quantitative estimates of LPS and tangential extension. LPS increases overall westward and toward the salient ends, from <5% in the central parts of the Hogsback system to 10%–30% in the Crawford system. Tangential extension is widespread but minor (≤5%). Strike tests for cleavage and strain directions have slopes of ~0.9, indicating LPS directions were about, but not precisely, perpendicular to structural trend. Strain patterns also reflect local structural complications. Areas with oblique structural trends near moderately dipping oblique ramps experienced limited vertical-axis rotations, whereas significant rotation likely occurred near steeply dipping tear faults. Interactions between the Sevier thrust belt and Laramide foreland uplifts varied with location, from local shear and transpression where frontal thrusts impinged on fault-bounded uplifts to tilting above arches that projected beneath the thrust belt.

Previous studies have also found systematic mesoscopic structural and strain patterns in parts of the Wyoming salient, although interpretations have varied. Crosby (1969) interpreted cleavage, minor folds, and contraction faults to reflect initially radial LPS directions, with no secondary rotation. In comparison, Craddock et al. (1988) interpreted variations in fracture patterns and calcite twin strain directions in the northern part of the salient to record curved deformation paths and rotation as each thrust sheet was emplaced. In the central part of the salient, Craddock (1992) interpreted cleavage and calcite

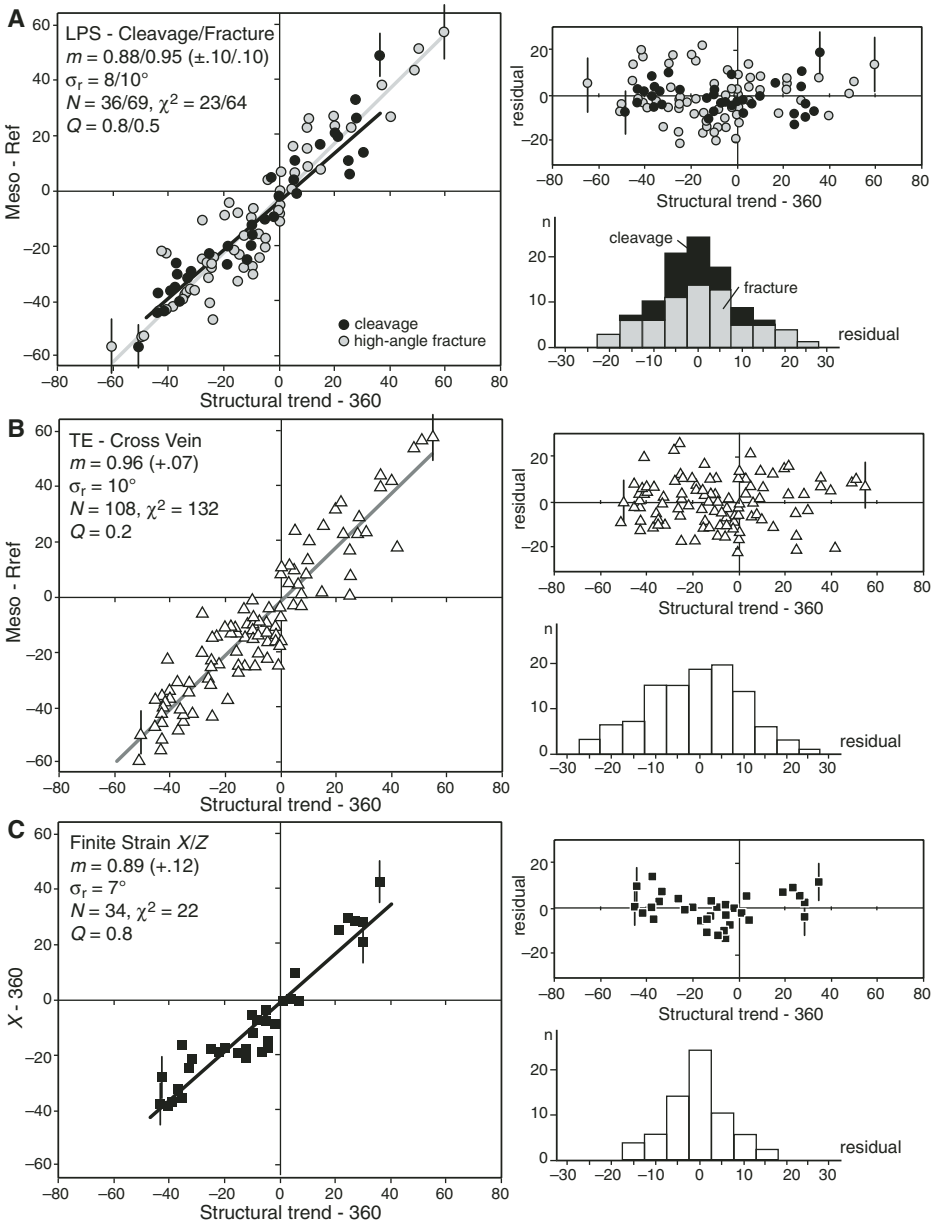

Figure 19. Strike-test results for deformation fabrics in the Ankareh Formation. (A) Plot of filtered layer-parallel shortening (LPS) directions (relative to a reference of 090°) estimated from cleavage (solid circles) and high-angle fracture sets (gray circles) versus structural trend (relative to a reference of 360°). Data show a strong correlation with best-fit slopes (*m*) of 0.88 and 0.95 for cleavage and fractures. Residuals are uncorrelated with trend and have normal distributions for both cleavage and fractures, but fractures display greater variance. (B) Plot of extension directions (relative to a reference of 360°) estimated from cross-strike veins and fractures versus structural trend. Data define a best-fit slope of 0.96 and 2σ (95%) confidence interval of ±0.07. Relations are similar to those in the Twin Creek Formation. (C) Plot of finite strain *X* directions (which are orthogonal to tectonic shortening directions) versus structural trend. Data show a strong correlation with a best-fit slope of 0.89 and 2σ (95%) confidence interval of ±0.12, consistent with the slope estimated from cleavage orientations.

twin strains to record initial E-W LPS directions that were subsequently rotated during dextral transpression. In the southern part of the salient, Bradley and Bruhn (1988) interpreted cleavage and vein patterns to reflect E-W wrench shear and tilting along the northern flank of the Uinta-Cottonwood Arch. Such varying interpretations, despite similarities in structural observations, partly result from lack of data on vertical-axis rotations needed to quantify initial LPS directions.

Mitra (1994) reported average LPS values of ~10%, 15%, and 25%, respectively, for parts of the Hogsback, Absaroka, and Crawford thrust systems, which are broadly similar to values for this study, and Gockley (1985) reported strain data for reduction spots in the Big Elk anticline that are similar to values shown in Figure 8B. This consistency between the extensive data sets reported here and previous local studies indicates that despite structural complexities, regional strain patterns can be deciphered by careful analysis.

Constraints on Kinematic Models

Regional patterns of internal strain constrain kinematic models of the Wyoming salient. A primary arc with uniform slip (model 1 in Fig. 2) predicts no rotation of linear LPS fabrics with a fabric strike-test slope of 0, no tangential extension, and parallel fault-slip lineations, inconsistent with observations. A primary arc with radial slip (model 2 in Fig. 2) predicts radial LPS directions with a strike-test slope of 1.0, major (>10%) tangential extension that increases progressively as thrust sheets are emplaced, and radial slip lineations. Although LPS directions define a radial pattern in the Wyoming salient, observed minor (≤5%) tangential extension and insignificant extension in wedge-top sedimentary deposits are inconsistent with this model. Secondary oroclines with superimposed wrench shear and bending (models 5 and 6 in Fig. 2) predict younger increments of internal strain and rotation that overprint older fold-and-thrust structures. Structural relations and timing constraints from synorogenic deposits, however, indicate that internal strain was closely associ-

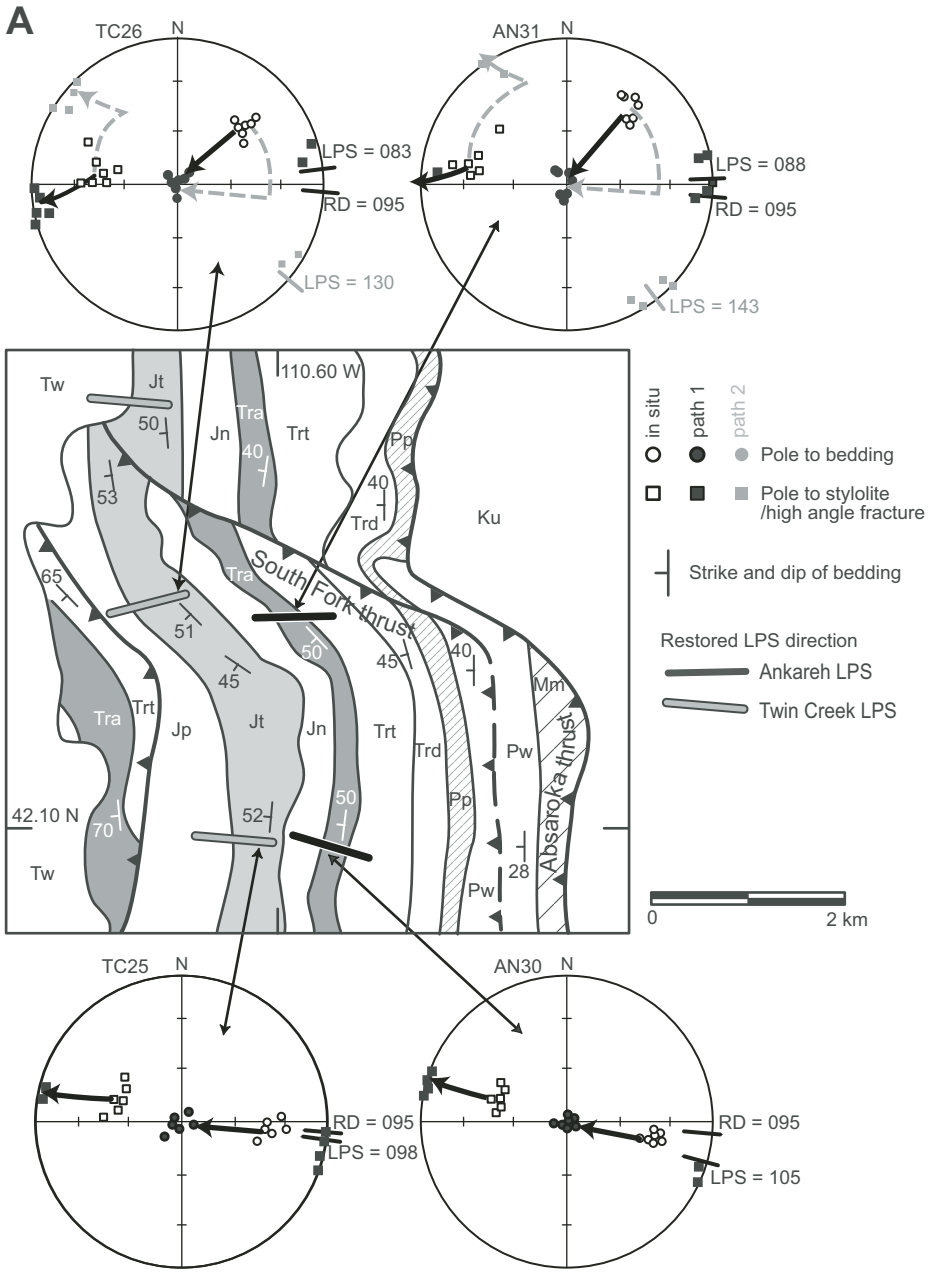

Figure 20 (*on this and following two pages*). Examples of relations in structurally complex areas. (A) Beaver Creek area with oblique ramp in the South Fork thrust (location BC in Fig. 3A). Stereograms show in situ and restored layer-parallel shortening (LPS) fabrics for two paths: 1—single rotation about bed strike (black), and 2—vertical-axis rotation followed by rotation about N-S bed strike (dashed gray). Path 1 gives restored E to ESE LPS directions consistent with a regional shortening direction (RD) of 095°, suggestive of limited (≤10°) rotation in area of oblique ramp. Geologic map is modified from Apotria (1995) and Rubey et al. (1980). Units are: Mm—Mississippian Madison Formation, Pw—Pennsylvanian Wells Formation, Pp—Permian Phosphoria Formation, Trd—Triassic Dinwoody and Woodside Formations, Trt—Thaynes Formation, Tra—Ankareh Formation, Jn—Jurassic Nugget Formation, Jt—Twin Creek Formation, Jp—Preuss Formation, Ku—Cretaceous strata undivided, and Tw—Tertiary Wasatch Formation deposited in wedge-top basin.

ated with large-scale folding and thrusting in the Wyoming salient. A progressive arc with parallel thrust slip and differential shortening (model 4 in Fig. 2) predicts variable rotation of LPS directions, wrench shear, and parallel slip lineations, partly consistent with observations. Fault-slip lineations in the salient, however, display spatial variations. A progressive arc with curved thrust slip and a component of primary curvature (model 3 in Fig. 2) predicts LPS directions about perpendicular to structural trend, minor but widespread tangential extension, and variable slip lineations, consistent with observations from the salient.

The amounts of primary curvature and secondary vertical-axis rotation, however, cannot be uniquely determined from deformation fabrics alone, as initial strain directions are uncertain. For example, a salient with a final trend of 040° to 320° and LPS directions of 130° to 050° could result from either: a progressive arc with 0% primary curvature, a constant initial trend of 000°, and a constant initial LPS direction of 090°, which undergoes 100% secondary rotation of ±40° (case 1, Fig. 21); or a primary arc that starts with 100% primary curvature, an initial trend of 040° to 320°, and radial LPS directions of 130°–050°, which then undergoes radial slip with 0% secondary rotation (case 2, Fig. 21). In both cases, LPS directions start and remain orthogonal to structural trend, yielding a strike test slope of 1.0, even though the amounts of secondary rotation are different. This ambiguity results from strain fabrics having variable initial directions related to primary curvature and stress/strain refraction, such that final directions do not directly record vertical-axis rotation.

Initial LPS directions can be quantified by integrating strain data with the distribution and timing of vertical-axis rotations determined by paleomagnetic studies. Cleavage and finite strain

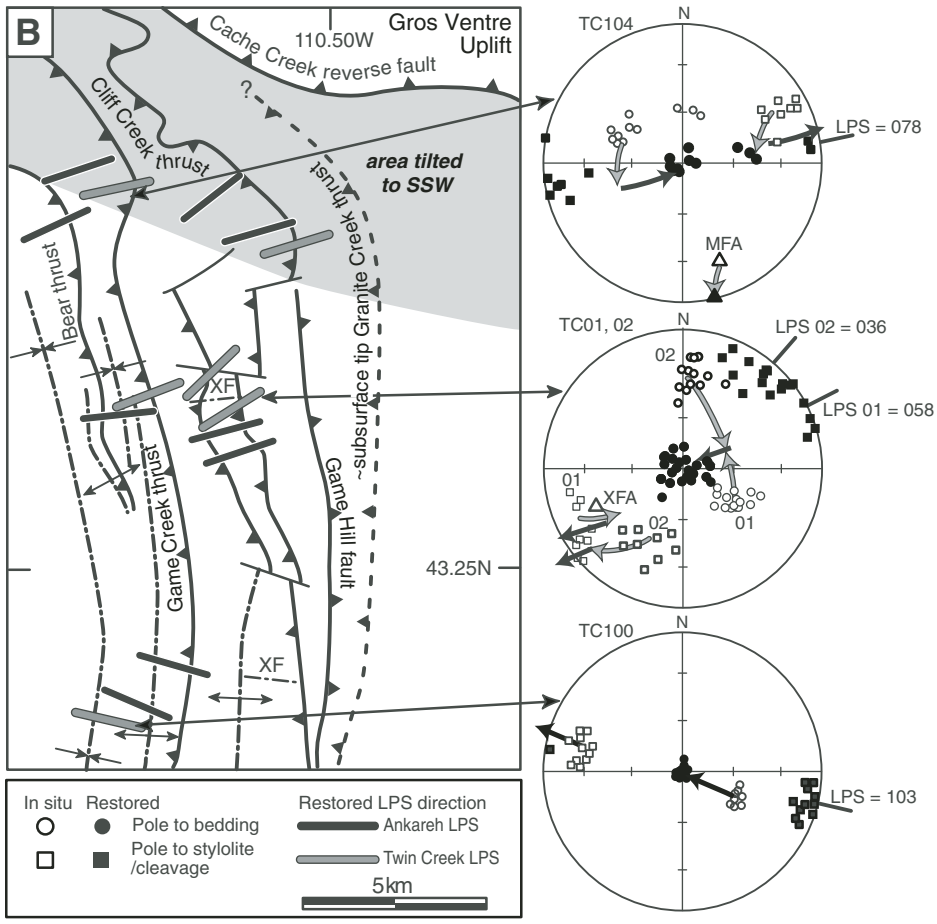

Figure 20 (*continued*). (B) Granite Creek area (location GC in Fig. 3A) where frontal thrusts interact with the Gros Ventre foreland uplift. Area tilted to SSW near the foreland uplift is shown by shaded pattern. Restored LPS directions in both the Twin Creek and Ankareh Formations are mostly ENE at high angles to the regional NNW structural trend, but they are rotated to ESE in the southern part of the area (site TC100) where slip on the subsurface Granite Creek thrust increases to the north. Stereograms for sites TC01 and TC02 illustrate cross folding about a WSW-plunging axis (XFA, limbs restored along gray path). Stereogram for site TC104 illustrates minor fold axis (MFA) and cleavage tilted near the Gros Ventre uplift (restored along gray path). Geologic map is modified from Hunter (1988).

directions yield a fabric strike-test slope of ~0.9, indicating early LPS directions were about, but not precisely, perpendicular to structural trend in the Wyoming salient. Paleomagnetic data define a regional strike-test slope of ~0.75, indicating an average of 75% secondary rotation and 25% primary curvature (Weil et al., 2009). These data are consistent with a progressive arc having an initial trend of 010°–350° and initial LPS directions of 096° to 084°, which then undergoes secondary rotation of ±30° to produce a salient with a final trend of 040° to 320° (case 3, Fig. 21). Note, LPS fabrics start with varying directions between E-W and orthogonal to structural trend. More internal thrust sheets experienced minor additional rotation during slip on frontal thrusts, which locally interacted with foreland uplifts at the salient ends.

Implications of Incorporating Internal Strain into Restorations

Average values of LPS in the central part of the salient range from ~5% in frontal parts of the Hogsback system to ~20% in the Crawford system. Restoration of large-scale thrusting and folding along section X-X′ (Fig. 4) gives an estimated 36 km of shortening for the Hogsback system (mostly from slip on the main frontal thrust), and an additional 3.8 km of internal shortening from 5% LPS over a bed length of 75 km (Fig. 22). In comparison, restoration of the Crawford system gives an estimated 8 km of shortening on the main thrust, 25 km of shortening by large-scale folds and imbricates, and an additional 12 km of internal shortening from 20% LPS over a bed length of 60 km (Fig. 22). Two main points are gleaned from these relations. (1) Internal strain accommodated significant shortening in the Crawford system but was minor in the Hogsback system. Taken across the thrust belt, LPS accounted for ~15% of total shortening in sections X-X′ and Y-Y′ (Fig, 4), which must be incorporated for accurate restoration and estimates of initial taper (Mitra, 1994). Note, LPS is greater in the Crawford system, even though this system has less slip on the main thrust, illustrating that internal strain and bulk translation are partly independent in thrust wedges (Elliott, 1976). (2) Total shortening (incorporating LPS) decreases from 140 to 95 km between sections X-X′ and Y-Y′, requiring vertical-axis rotation and/or wrench shear to accommodate gradients in displacement. Using a strike length of 150 km between sections, this difference in total shortening could be accommodated by 20° clockwise rotation in the southern part of the salient, consistent with paleomagnetic data (Weil et al., 2009).

Strain compatibility between stratigraphic levels is another important factor for balancing cross sections. Magnitudes and directions of LPS are broadly similar in the Ankareh and Twin Creek Formations (Figs. 13 and 17), and for other formations (Mitra, 1994). However, detachments of various scales locally transfer shortening between levels. Detachments in Devonian and Lower Triassic strata separate packages that deformed mostly by imbricate faulting at deeper levels and detachment folding at shallower levels in the Big Elk anticline, though total shortening is similar between levels (Banerjee and Mitra, 2005). In contrast, a detachment in Upper Jurassic evaporites transferred shortening from folded Triassic to Middle Jurassic strata regionally eastward into folded Cretaceous strata within parts of the Absaroka system (Fig. 20C; Coogan and Yonkee, 1985). Thus, strain patterns and characteristics of detachment systems that transfer shortening between structural levels must be integrated for viable restorations.

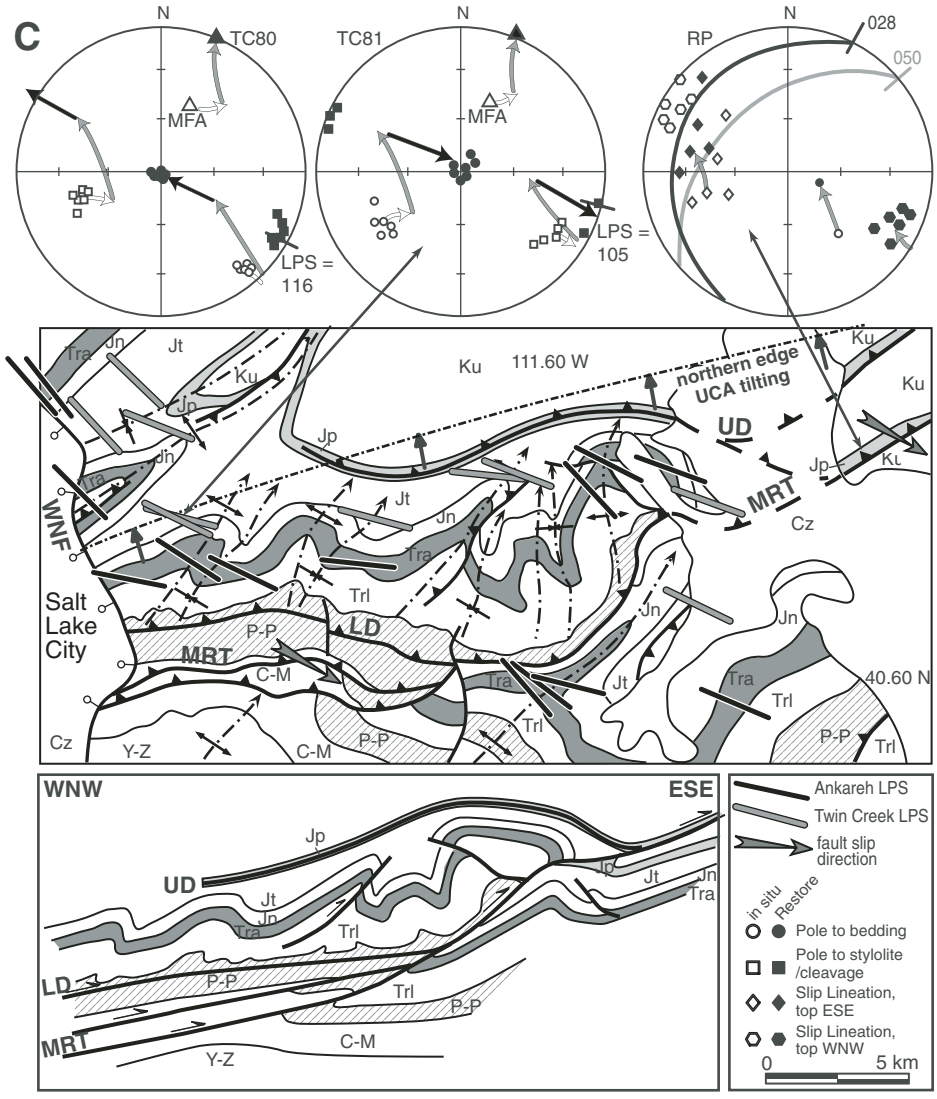

Figure 20 (*continued*). (C) Parleys Canyon area (location PC in Fig. 3A) where Absaroka thrust system is tilted by foreland Uinta-Cottonwood Arch (UCA) and in footwall of Wasatch normal fault (WNF). Down-plunge projection illustrates relations between Mount Raymond thrust (MRT), and lower and upper detachments (LD and UD) in Permian and Jurassic strata. Stereograms for sites TC80 and TC81 along limbs of minor fold show restoration of cleavage by removing tilting in footwall of WNF (white path), tilting by the Uinta-Cottonwood Arch (gray), and unfolding limbs (black). Restored LPS directions in the Ankareh and Twin Creek Formations trend consistently ESE at high angles to fold axial traces. Slip lineations on minor faults along the Mount Raymond thrust in the Rockport area (site RP) record ESE-WNW slip after restoration of tilting along the Uinta-Cottonwood Arch (gray path). Currently, the fault strikes 050° and dips moderately NW (gray great circle), but after restoration, it has a strike of 028° and dips gently WNW (black great circle). Units are: YZ—Meso/Neoproterozoic rocks, C-M—Cambrian to Mississippian strata, P-P—Pennsylvanian to Permian strata, Trl—Lower Triassic strata, Tra—Ankareh Formation, Jn—Jurassic Nugget Formation, Jt—Twin Creek Formation, Jp—Preuss Formation, Ku—Cretaceous strata, undivided, Cz—Cenozoic deposits. Geologic map is modified from Bryant (1992).

Spatial and Temporal Evolution of LPS Fabrics

Regional strain, structural, and stratigraphic relations constrain the temporal and spatial evolution of LPS fabrics during thrusting in the Wyoming salient. Within the Crawford system, the dominant cleavage continues westward and becomes more intense near footwall imbricates of the Meade thrust. Here, cleavage is acute to bedding in a footwall syncline and at low angles to the Meade thrust, indicating concurrent development (Mitra et al., 1988). Cleavage, however, is strongly fanned about large-scale folds that developed during slip on the Crawford system (Fig. 8). Gently dipping Late Cretaceous strata lie with angular unconformity over folded rocks of the Crawford system and display only limited internal strain; these strata were deposited in local wedge-top basins, synchronous with major slip on the Absaroka thrust system to the east (Coogan, 1992; Yonkee et al., 1997). Thus, LPS fabrics in the Crawford system developed largely during Early Cretaceous emplacement of the Willard and Meade thrusts, followed by middle Cretaceous thrusting, and then by mostly passive transport during the Late Cretaceous as the thrust front propagated eastward. Cleavage intensity and strain ratios are high to moderate in the Crawford system, but they decrease eastward, indicating that LPS was concentrated in an ~60-km-wide belt (restored length prior to Crawford thrusting) in front of the Willard and Meade thrusts. Early Cretaceous emplacement of the Willard and Meade thrusts and deposition of thick foredeep sediments increased burial depths, temperatures, and rates of pressure solution within the future Crawford system (Mitra and Yonkee, 1985; DeCelles et al., 1993).

Within central parts of the Hogsback system, cleavage is absent, and shortening is mostly by large-scale thrust slip. Cleavage intensity, however, increases westward in folds associated with footwall imbricates of the Absaroka thrust (Fig. 13). Thus, cleavage in the Hogsback system likely developed mostly during Late Cretaceous slip on the Absaroka thrust. Cleavage intensity and strain also increase toward the northern end of the Hogsback system, which is interpreted to record buttressing by foreland uplifts that impeded thrust slip and increased local stress.

A conceptual model for the evolution of deformation fabrics in the Wyoming salient is illustrated in Figure 23. In this model, a main cleavage formed during early LPS in each thrust system, related to: (1) increases in temperatures and burial depths during emplacement of overriding thrust sheets and foredeep sedimentation; and (2) increases in deviatoric stress near footwall

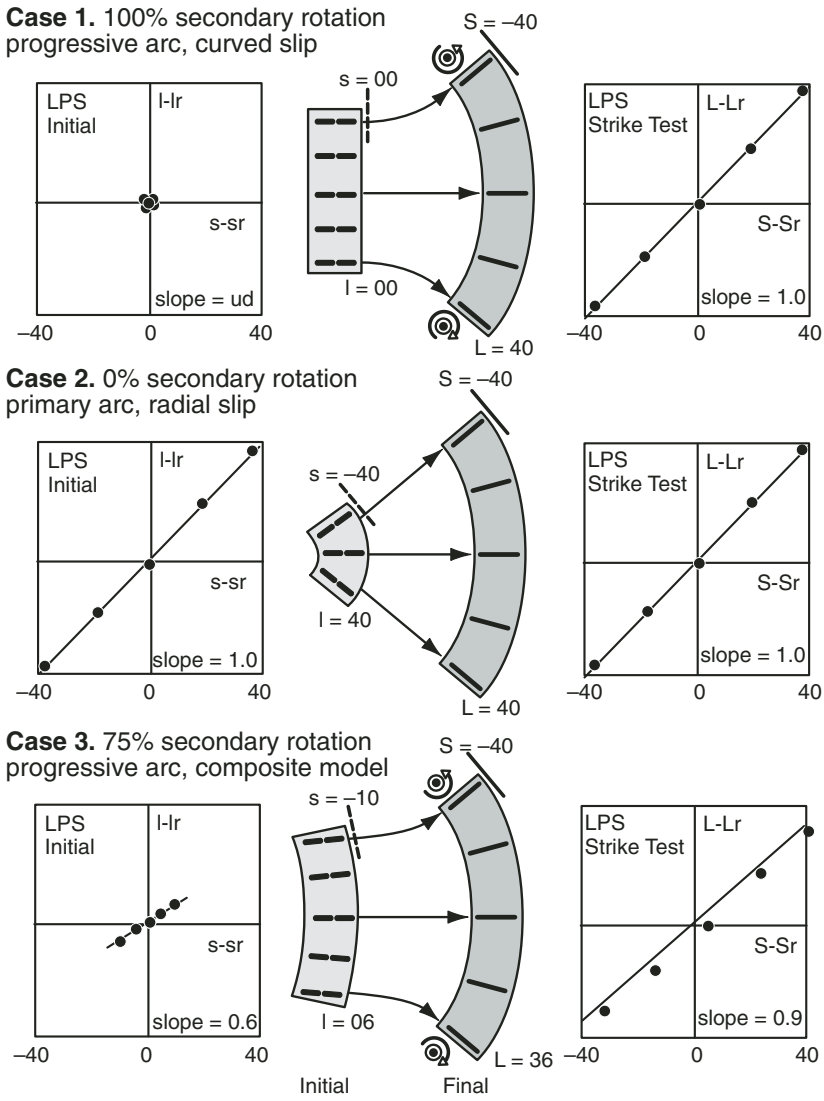

Figure 21. Idealized cases for variations in initial and final layer-parallel shortening (LPS) directions (l and L) and structural trend (s and S) around a salient. Case 1 starts with a linear belt (0% primary curvature) and uniform LPS directions, which then undergo 100% secondary rotation. Case 2 starts with a primary arc (100% primary curvature) and orthogonal LPS directions, which then undergo radial slip with 0% secondary rotation. In both cases, the final strike-test slope is 1.0. Unless initial LPS directions are known, secondary rotation cannot be uniquely determined. Case 3 illustrates a simplified kinematic model for the Wyoming salient with primary curvature of 10° in structural trend and initial variation of ±6° in LPS fabrics, which are subsequently rotated by 30°.

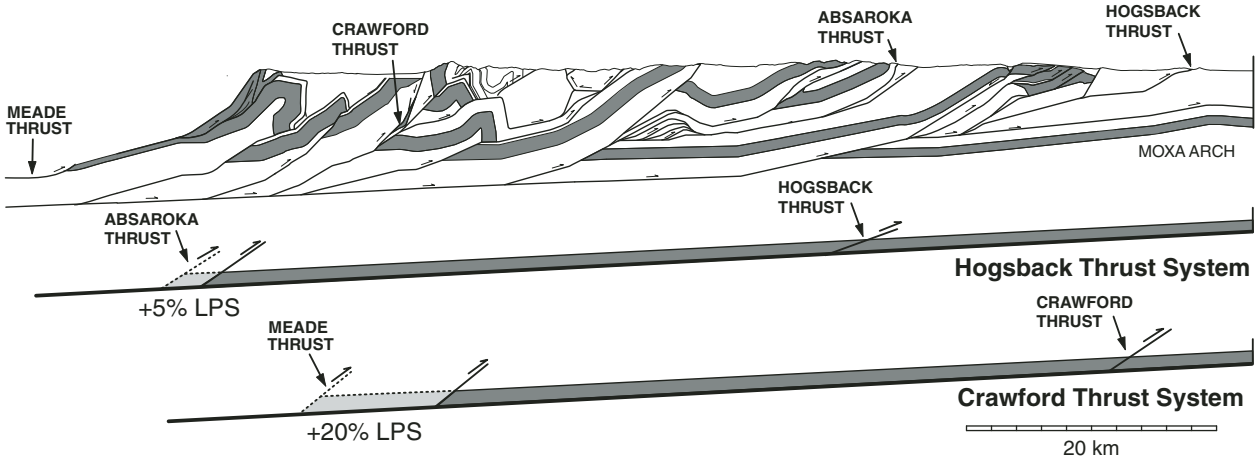

Figure 22. Restoration of Triassic strata for the Hogsback and Crawford thrust systems along section X-X′ from Figure 4. Early layer-parallel shortening (LPS) accounts for minor shortening in the Hogsback system but is an important component of total shortening in the Crawford system. Note, shortening from footwall imbricates of the Meade thrust is not included in the Crawford restoration.

imbricates along the leading edge of the growing thrust wedge. Early LPS directions had minor variations around the salient, likely reflecting a component of topographically induced deviatoric stress along the curved front of the thrust wedge, similar to observed stress variations along the active front of the Andean retro-arc belt (Guzman et al., 2007). As deformation progressed, areas in front of the wedge were incorporated into foreland propagating thrust systems. Each thrust system underwent secondary rotation during curved fault slip, which rotated early LPS fabrics, producing the observed radial patterns. Minor tangential extension and wrench shear accompanied thrusting, resulting in development of veins and tear faults over a protracted history. Although LPS was concentrated near the leading edge of the growing wedge, minor orogenic stresses may have extended into the foreland where they interacted with far field stresses in the plate interior (Bird, 2002). For example, Craddock and van der Pluijm (1999) interpreted calcite twinning strains in Cretaceous strata from Minnesota as recording stresses related to the Sevier-Laramide orogeny, with estimated stress magnitudes decreasing eastward into the plate interior (van der Pluijm et al., 1997).

During growth of the wedge, structural style evolved within developing thrust systems (Fig. 23B). Earliest deformation resulted in calcite twinning strains that extended into the foreland and accumulated at very low stresses. Because twinning typically causes strain hardening, these strains are limited but may preserve a record of initial stress trajectories (Craddock, 1992). A main period of LPS occurred as burial depths, and deviatoric stress increased in front of the growing thrust wedge, forming cleavage, small-scale buckle folds, and minor faults. Subsequently, large-scale thrusting and folding occurred as deformation became more discrete, possibly due to increasing fluid pressure, clay alteration, and grain-size reduction along weakening fault zones. Surface thrusting then propagated toward the foreland, while internal thrust sheets were passively transported and critical taper decreased toward the hinterland. Higher taper near the leading edge of the wedge resulted in larger components of topographically induced stress and greater curvature in stress directions, leading to curved fault slip and vertical-axis rotation concentrated along the active wedge front. These patterns reflect interacting processes that produced curvature in the Wyoming salient, including variations in thickness of the initial sedimentary prism and subsequent foredeep deposits, variations in fault strength, and interaction with foreland uplifts, as more thoroughly explored in the companion paper by Weil et al. (2009).

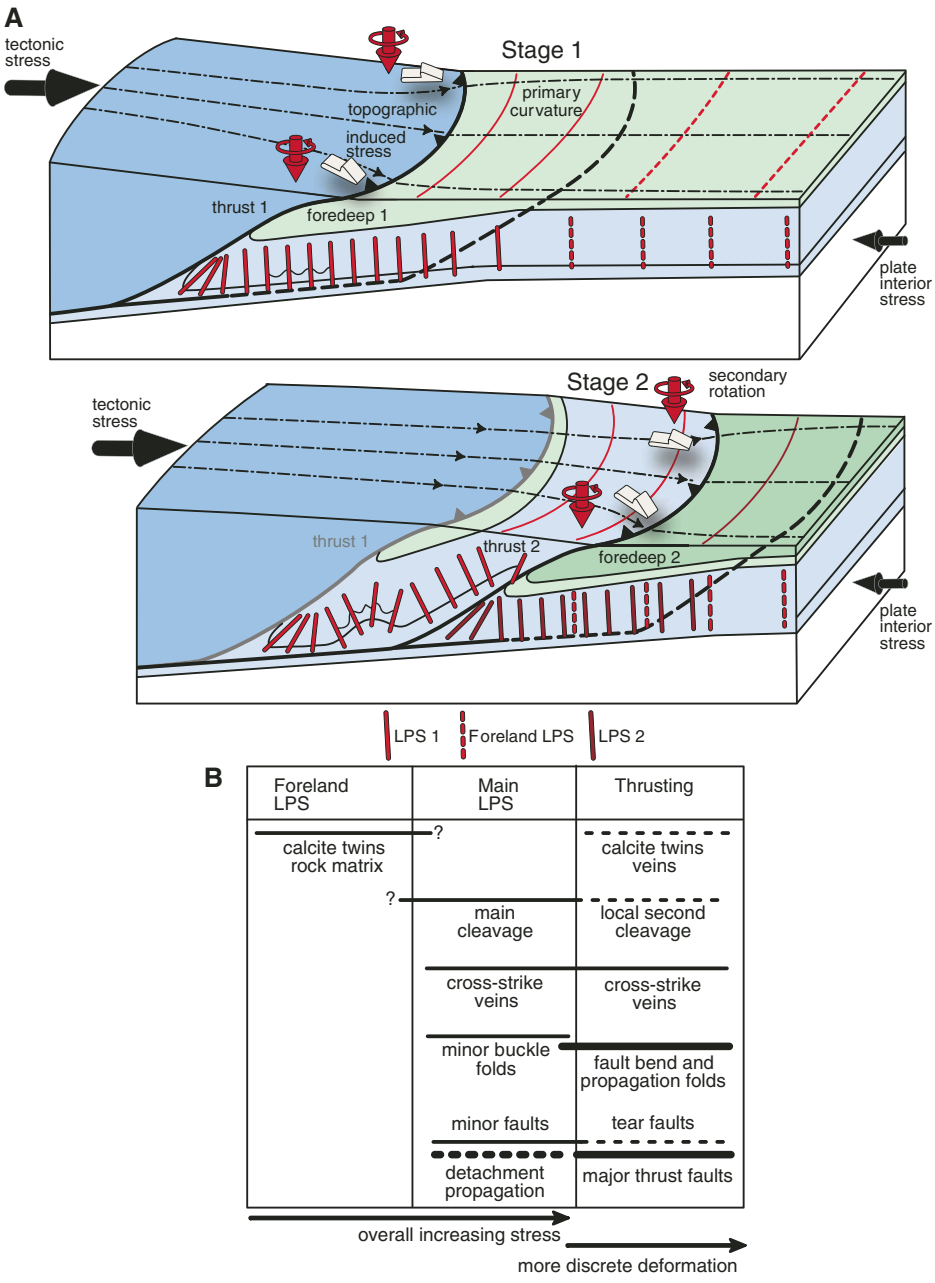

Figure 23. (A) Model for development of layer-parallel shortening (LPS) fabrics during progressive growth of the Sevier thrust wedge. Stage 1: Early LPS fabrics (solid red lines) develop during increased burial and stress in front of the main active thrust. LPS directions have primary curvature related to a component of topographically induced stress along the curved front of the thrust wedge (idealized σ_1 trajectories indicated by dot-dash lines). Incipient LPS fabrics (dashed red lines) may extend farther into the foreland, where they are influenced by plate interior stresses. Stage 2: A second thrust propagates as the wedge grows. Early LPS fabrics are fanned about large-scale folds and also undergo vertical-axis rotation during curved thrust slip. The interior thrust sheet is mostly passively transported, and taper decreases as the basal décollement weakens. A second LPS fabric (brown lines) develops in front of the wedge and may overprint earlier foreland LPS fabrics. (B) Diagram of idealized temporal evolution in structural style as an area moves from being in the distal foreland, to in front of the orogenic wedge, to being incorporated into the wedge.

CONCLUSIONS

1. The Wyoming salient displays distinctly curved structural trends associated with varying thrust slip directions, changes in fold-and-thrust shortening, and interaction with foreland uplifts.

2. Thrust systems have systematic suites of mesoscopic structures to grain-scale fabrics that accommodated early LPS, tangential extension, minor wrench shear, and layer-parallel shear.

3. Strain analysis in limestone and red beds indicates that internal shortening increased westward and toward the salient ends, with <5% LPS in central parts of the Hogsback system to 10%–30% LPS in the more interior Crawford system.

4. LPS directions were about (but not precisely) perpendicular to structural trend within thrust systems. This radial pattern likely reflects secondary rotation along with a component of primary curvature related to stress variations near the leading edge of the thrust wedge.

5. Internal strain patterns are consistent with progressive secondary rotation produced by curved thrust slip and differential shortening. Quantification of secondary rotation, however, requires integrating paleomagnetic data.

6. Strain was an important part of the total deformation field in more interior sheets, and must be considered for accurate restoration of cross sections. By integrating strain, paleomagnetic, and regional structural studies, limitations of each data set can be overcome to develop three-dimensional kinematic models of orogenic curvature.

7. Early LPS was concentrated in front of the growing thrust wedge, related to increases in temperature and burial during emplacement of overriding thrust sheets and foredeep sedimentation and to increased deviatoric stress near propagating footwall imbricates.

ACKNOWLEDGMENTS

This work was supported by National Science Foundation (NSF) grants EAR-0409103 and EAR-0408653. Many students from Bryn Mawr College, Haverford College, and Weber State University participated in field and laboratory work, which greatly enhanced the quality of this study. These students were Tyler Cluff, Andrea Cutruzzula, Steve Fellows, Melissa Lindholm, Anna Mazzariello, Sarah McCullough, Evan Pugh, Zoe Ruge, Cameron Thompson, Matt Tomich, Kira Tushman, and Virginia Walker. Insightful reviews by Pete DeCelles, John Craddock, and Stephen Johnston significantly improved this paper.

REFERENCES CITED

Allerton, S., 1998, Geometry and kinematics of vertical-axis rotations in fold and thrust belts: Tectonophysics, v. 299, p. 15–30, doi: 10.1016/S0040-1951(98)00196-6.

Apotria, T.G., 1995, Thrust sheet rotation and out-of-plane strains associated with oblique ramps; an example from the Wyoming salient, U.S.A.: Journal of Structural Geology, v. 17, p. 647–662, doi: 10.1016/0191-8141(94)00087-G.

Armstrong, F.C., and Oriel, S.S., 1965, Tectonic development of the Idaho-Wyoming thrust belt: American Association of Petroleum Geologists Bulletin, v. 49, p. 1847–1866.

Armstrong, R.L., 1968, Sevier orogenic belt in Nevada and Utah: Geological Society of America Bulletin, v. 79, p. 429–458.

Banerjee, S., and Mitra, S., 2005, Fold-thrust styles in the Absaroka thrust sheet, Caribou National Forest area, Idaho-Wyoming thrust belt: Journal of Structural Geology, v. 27, p. 51–65, doi: 10.1016/j.jsg.2004.07.004.

Bayona, G., Thomas, W.A., and Van der Voo, R., 2003, Kinematics of thrust sheets within transverse zones: A structural and paleomagnetic investigation in the Appalachian thrust belt of Georgia and Alabama: Journal of Structural Geology, v. 25, p. 1193–1212, doi: 10.1016/S0191-8141(02)00162-1.

Beutner, E.C., 1977, Causes and consequences of curvature in the Sevier orogenic belt, Utah to Montana, *in* Helsey, E.L., Lawson, D.E., Norwal, E.R., Wach, P.H., and Hale, L.E., eds., Rocky Mountain Thrust Belt, Geology and Resources: Wyoming Geological Association Guidebook, v. 29, p. 353–365.

Bird, P., 2002, Stress direction history of the western United States and Mexico since 85 Ma: Tectonics, v. 21, doi: 10.1029/2001TC001319.

Blackstone, D., 1977, The Overthrust Belt salient of the Cordilleran fold belt, western Wyoming, southeastern Idaho, northeastern Utah: Wyoming Geological Association Guidebook, v. 29, p. 367–384.

Bradley, M.D., and Bruhn, R.L., 1988, Structural interactions between the Uinta Arch and the Overthrust Belt, north-central Utah; implications of strain trajectories and displacement modeling, *in* Schmidt, C.J., and Perry, W.J., eds., Interaction of the Rocky Mountain Foreland and the Cordilleran Thrust Belt: Geological Society of America Memoir 171, p. 431–445.

Bryant, B., 1992, Geologic Map of the Salt Lake City 30′ × 60′ Quadrangle, North-Central Utah and Uinta County, Wyoming: U.S. Geological Survey Map I-1944, scale 1:100,000.

Burtner, R.L., and Nigrini, A., 1994, Thermochronology of the Idaho-Wyoming thrust belt during the Sevier orogeny; a new, calibrated, multiprocess thermal model: American Association of Petroleum Geologists Bulletin, v. 78, p. 1586–1612.

Butler, R.F., Richards, D.R., Sempere, T., and Marshall, L.G., 1995, Paleomagnetic determinations of vertical-axis tectonic rotations from Late Cretaceous and Paleocene strata of Bolivia: Geology, v. 23, p. 799–802, doi: 10.1130/0091-7613(1995)023<0799:PDOVAT>2.3.CO;2.

Carey, S.W., 1955, The orocline concept in geotectonics: Proceedings of the Royal Society of Tasmania, v. 89, p. 255–288.

Conder, J., Butler, R.F., DeCelles, P.G., and Constenius, K.N., 2003, Paleomagnetic determination of vertical-axis rotations in the Charleston-Nebo salient, Utah: Geology, v. 31, p. 1113–1116, doi: 10.1130/G19893.1.

Coogan, J.C., 1992, Structural evolution of piggyback basins in the Wyoming-Idaho-Utah thrust belt, *in* Link, P.K., Kuntz, M.A., and Platt, L.B., eds., Regional Geology of Eastern Idaho and Western Wyoming: Geological Society of America Memoir 179, p. 55–81.

Coogan, J.C., and Yonkee, W.A., 1985, Salt detachments in the Jurassic Preuss Formation within the Meade and Crawford thrust systems, Idaho and Wyoming, *in* Kearns, G.J., and Kearns, R.L., eds., Orogenic Patterns and Stratigraphy of North-Central Utah and Southeastern Idaho: Utah Geological Association Publication 14, p. 75–82.

Craddock, J.P., 1992, Transpression during tectonic evolution of the Idaho-Wyoming fold-and-thrust belt, *in* Link P.K., Kuntz, M.A., and Platt, L.B., eds., Regional Geology of Eastern Idaho and Western Wyoming: Geological Society of America Memoir 179, p. 125–139.

Craddock, J.P., and van der Pluijm, B., 1999, Sevier-Laramide deformation of the continental interior from calcite twinning analysis, west-central North America: Tectonophysics, v. 305, p. 275–286, doi: 10.1016/S0040-1951(99)00008-6.

Craddock, J.P., Kopania, A.A., and Wiltschko, D.V., 1988, Interaction between the northern Idaho-Wyoming thrust belt and bounding basement blocks, central western Wyoming, *in* Schmidt, C.J., and Perry, W.J., Jr., eds., Interaction of the Rocky Mountain Foreland and the Cordilleran Thrust Belt: Geological Society of America Memoir 171, p. 333–351.

Crosby, G.W., 1969, Radial movements in the western Wyoming salient of the Cordilleran Overthrust Belt: Geological Society of America Bulletin, v. 80, p. 1061–1077, doi: 10.1130/0016-7606(1969)80[1061:RMITWW]2.0.CO;2.

Dahlstrom, C.D.A., 1969, Balanced cross sections: Canadian Journal of Earth Sciences, v. 6, p. 743–757.

DeCelles, P.G., 1994, Late Cretaceous–Paleocene synorogenic sedimentation and kinematic history of the Sevier thrust belt, northeast Utah and southwest Wyoming: Geological Society of America Bulletin, v. 106, p. 32–56, doi: 10.1130/0016-7606(1994)106<0032:LCPSSA>2.3.CO;2.

DeCelles, P.G., 2004, Late Jurassic to Eocene evolution of the Cordilleran thrust belt and foreland basin system, western U.S.A.: American Journal of Science, v. 304, p. 105–168, doi: 10.2475/ajs.304.2.105.

DeCelles, P.G., and Mitra, G., 1995, History of the Sevier orogenic wedge in terms of critical taper models, northeast Utah and southwest Wyoming: Geological Society of America Bulletin, v. 107, p. 454–462, doi: 10.1130/0016-7606(1995)107<0454:HOTSOW>2.3.CO;2.

DeCelles, P.G., Pile, H.T., and Coogan, J.C., 1993, Kinematic history of the Meade thrust based on provenance of the Bechler Conglomerate at Red Mountain, Idaho, Sevier thrust belt: Tectonics, v. 12, p. 1436–1450.

Dixon, J.S., 1982, Regional structural synthesis, Wyoming salient of the western Overthrust Belt: American Association of Petroleum Geologists Bulletin, v. 10, p. 1560–1580.

Dorr, J.A., Spearing, D.R., and Steidtmann, J.R., 1977, Deformation and deposition between a foreland uplift and an impinging thrust belt; Hoback Basin, Wyoming: Geological Society of America Special Paper 177, 82 p.

Elliott, D., 1976, The motion of thrust sheets: Journal of Geophysical Research, v. 81, p. 949–963, doi: 10.1029/JB081i005p00949.

Ferrill, D.A., and Groshong, R.A., Jr., 1993, Model for kinematic curvature of the northern Subalpine Chain, France: Journal of Structural Geology, v. 15, p. 523–541, doi: 10.1016/0191-8141(93)90146-2.

Geiser, P.A., and Engelder, T., 1983, The distribution of layer parallel shortening fabrics in the Appalachian foreland of New York and Pennsylvania; evidence for two noncoaxial phases of the Alleghanian orogeny, *in* Hatcher, R.D., Jr., et al., eds., Contributions to the Tectonics and Geophysics of Mountain Chains: Geological Society of America Memoir 158, p. 161–175.

Gockley, C.K., 1985, Structure and Strain Analysis of the Big Elk Mountain Anticline, Caribou Mountains, Idaho [M.S. thesis]: Boulder, University of Colorado, 112 p.

Gray, M.B., and Stamatakos, J., 1997, New model for evolution of fold and thrust belt curvature, based on integrated structural and paleomagnetic results from the Pennsylvania salient: Geology, v. 25, p. 1067–1070, doi: 10.1130/0091-7613(1997)025<1067:NMFEOF>2.3.CO;2.

Grubbs, K.L., and Van der Voo, R., 1976, Structural deformation of the Idaho-Wyoming Overthrust Belt (U.S.A.), as determined by Triassic paleomagnetism: Tectonophysics, v. 33, p. 321–336, doi: 10.1016/0040-1951(76)90151-7.

Guzman, C., Cristallini, E., and Bottesi, G., 2007, Contemporary stress orientations in the Andean retroarc between 34 degrees S and 39 degrees S from borehole breakout analysis: Tectonics, v. 26, doi: 10.1029/2006TC001958.

Hext, G.R., 1963, The estimation of second-order tensors, with related tests and designs: Biometrika, v. 50, p. 353–373.

Hindle, H., and Burkhard, M., 1999, Strain, displacement and rotation associated with the formation of curvature

on fold belts; the example of the Jura arc: Journal of Structural Geology, v. 21, p. 1089–1101, doi: 10.1016/S0191-8141(99)00021-8.

Hnat, J.S., van der Pluijm, B.A., Van der Voo, R., and Thomas, W.T., 2008, Differential displacement and rotation in thrust fronts: A magnetic, calcite twinning and palinspastic study of the Jones Valley thrust, Alabama, US Appalachians: Journal of Structural Geology, v. 30, p. 725–738, doi: 10.1016/j.jsg.2008.01.012.

Hobbs, W.H., 1914, Mechanics of formation of arcuate mountains: The Journal of Geology, v. 22, p. 71–90.

Hogan, J.P., and Dunne, W.M., 2001, Calculation of shortening due to outcrop-scale deformation and its relation to regional deformation patterns: Journal of Structural Geology, v. 23, p. 1508–1529, doi: 10.1016/S0191-8141(01)00016-5.

Hunter, R.B., 1988, Timing and structural interaction between the thrust belt and foreland, Hoback Basin, Wyoming, *in* Schmidt, C.J., and Perry, W.J., eds., Interaction of the Rocky Mountain Foreland and the Cordilleran Thrust Belt: Geological Society of America Memoir 171, p. 431–445.

Imlay, R.W., 1967, Twin Creek Limestone (Jurassic) in the Western Interior of the United States: U.S. Geological Survey Professional Paper, 105 p.

Kley, J., and Monaldi, C.R., 1998, Tectonic shortening and crustal thickness in the Andes: How good is the correlation?: Geology, v. 26, p. 723–726, doi: 10.1130/0091-7613(1998)026<0723:TSACTI>2.3.CO;2.

Kollmeier, J.M., van der Pluijm, B.A., and Van der Voo, R., 2000, Analysis of Variscan dynamics; early bending of the Cantabria-Asturias Arc, northern Spain: Earth and Planetary Science Letters, v. 181, p. 203–216, doi: 10.1016/S0012-821X(00)00203-X.

Kummel, B., 1954, Triassic stratigraphy of southeastern Idaho and adjacent areas [Wyoming-Montana]: U.S. Geological Survey Professional Paper P 0254-H, p. 165–194.

Kwon, S., and Mitra, G., 2004, Strain distribution, strain history, and kinematic evolution associated with the formation of arcuate salients in fold-thrust belts; the example of the Provo salient, Sevier orogen, Utah, *in* Sussman, A.J., and Weil, A.B., eds., Orogenic Curvature—Integrating Paleomagnetic and Structural Analyses: Geological Society of America Special Paper 383, p. 205–223.

Lammerson, P., 1982, The Fossil Basin area and its relationship to the Absaroka thrust fault system, *in* Powers, R.B., ed., Geologic Studies of the Cordilleran Thrust Belt: Rocky Mountain Association of Geologists Publication, v. 1, p. 279–340.

Lawton, T.F., Boyer, S.E., and Schmitt, J.G., 1994, Influence of inherited taper on structural variability and conglomerate distribution, Cordilleran fold and thrust belt, western United States: Geology, v. 22, p. 339–342, doi: 10.1130/0091-7613(1994)022<0339:IOITOS>2.3.CO;2.

Lickorish, W.H., Ford, M., Buergisser, J., and Cobbold, P.R., 2002, Arcuate thrust systems in sandbox experiments; a comparison to the external arcs of the Western Alps: Geological Society of America Bulletin, v. 114, p. 1089–1107.

Macedo, J., and Marshak, S., 1999, Controls on the geometry of fold-thrust belt salients: Geological Society of America Bulletin, v. 111, p. 1808–1822, doi: 10.1130/0016-7606(1999)111<1808:COTGOF>2.3.CO;2.

Mansfield, G.R., 1927, Geography, Geology, and Mineral Resources of Part of Southeastern Idaho: U.S. Geological Professional Paper 152, 453 p.

Marshak, S., 1988, Kinematics of orocline and arc formation in thin-skinned orogens: Tectonics, v. 7, p. 73–86.

Marshak, S., 2004, Salients, recesses, arcs, oroclines, and syntaxes; a review of ideas concerning the formation of map-view curves in fold-thrust belts, *in* McClay, K.R., ed., Thrust Tectonics and Hydrocarbon Systems: American Association of Petroleum Geologists Memoir 82, p. 131–156.

Marshak, S., Wilkerson, M.S., and Hsui, A.T., 1992, Generation of curved fold-thrust belts: Insights from simple physical and analytical models, *in* McClay, K.R., ed., Thrust Tectonics: London, Chapman and Hall, p. 83–92.

McCaig, A.M., and McClelland, E., 1992, Palaeomagnetic techniques applied to thrust belts, *in* McClay, K.R., ed., Thrust Tectonics: London, Chapman and Hall, p. 209–216.

McNaught, M.A., and Mitra, G., 1996, The use of finite strain data in constructing a retrodeformable cross-section of the Meade thrust sheet, southeastern Idaho, U.S.A.: Journal of Structural Geology, v. 18, p. 573–583, doi: 10.1016/S0191-8141(96)80025-3.

McWhinnie, S.T., van der Pluijm, B.A., and Van der Voo, R., 1990, Remagnetizations and thrusting in the Idaho-Wyoming Overthrust Belt: Journal of Geophysical Research, v. 95, p. 4551–4559, doi: 10.1029/JB095iB04p04551.

Mitra, G., 1994, Strain variation in thrust sheets across the Sevier fold-and-thrust belt (Idaho-Utah-Wyoming); implications for section restoration and wedge taper evolution: Journal of Structural Geology, v. 16, p. 585–602, doi: 10.1016/0191-8141(94)90099-X.

Mitra, G., and Yonkee, W.A., 1985, Spaced cleavage and its relationship to folds and thrusts in the Idaho-Utah-Wyoming thrust belt of the Rocky Mountain Cordilleras: Journal of Structural Geology, v. 7, p. 361–373, doi: 10.1016/0191-8141(85)90041-0.

Mitra, G., Yonkee, W.A., and Gentry, D., 1984, Solution cleavage and its relationship to major structures in the Idaho-Utah-Wyoming thrust belt: Geology, v. 12, p. 354–358, doi: 10.1130/0091-7613(1984)12<354:SCAIRT>2.0.CO;2.

Mitra, G., Hull, J.M., Yonkee, W.A., and Protzman, G.M., 1988, Comparison of mesoscopic and microscopic deformational styles in the Idaho-Wyoming thrust belts and Rocky Mountain foreland, *in* Schmidt, C.J., and Perry, W.J., eds., Interaction of the Rocky Mountain Foreland and the Cordilleran Thrust Belt: Geological Society of America Memoir 171, p. 119–141.

Muttoni, G., Argnani, A., Kent, D.V., Abrahamsen, N., and Cibin, U., 1998, Paleomagnetic evidence for Neogene tectonic rotations in the northern Apennines, Italy: Earth and Planetary Science Letters, v. 154, p. 25–40, doi: 10.1016/S0012-821X(97)00183-0.

Nakamura, N., and Borradaile, G., 2001, Do reduction spots predate finite strain? A magnetic diagnosis of Cambrian slates in North Wales: Tectonophysics, v. 340, p. 133–139, doi: 10.1016/S0040-1951(01)00143-3.

Ong, P.F., van der Pluijm, B.A., and Van der Voo, R., 2007, Early rotation and late folding in the Pennsylvania salient (U.S. Appalachians); evidence from calcite-twinning analysis of Paleozoic carbonates: Geological Society of America Bulletin, v. 119, p. 796–804, doi: 10.1130/B26013.1.

Oriel, S.S., and Platt, L.B., 1980, Geologic Map of the Preston 1 × 2 Minute Quadrangle, Southeastern Idaho and Western Wyoming: U.S. Geological Professional Map I-1127, scale 1:250,000.

Owens, W.H., 1984, The calculation of a best-fit ellipsoid from elliptical sections on arbitrarily orientated planes: Journal of Structural Geology, v. 6, p. 571–578, doi: 10.1016/0191-8141(84)90066-X.

Paulsen, T., and Marshak, S., 1997, Structure of the Mount Raymond transverse zone at the southern end of the Wyoming salient, Sevier fold-thrust belt, Utah: Tectonophysics, v. 280, p. 199–211, doi: 10.1016/S0040-1951(97)00205-9.

Paulsen, T., and Marshak, S., 1999, Origin of the Uinta recess, Sevier fold-thrust belt: Influence of basin architecture on fold-thrust belt geometry: Tectonophysics, v. 312, p. 203–216, doi: 10.1016/S0040-1951(99)00182-1.

Protzman, G.M., and Mitra, G., 1990, Strain fabric associated with the Meade thrust sheet; implications for cross-section balancing: Journal of Structural Geology, v. 12, p. 403–417, doi: 10.1016/0191-8141(90)90030-3.

Pueyo, E.L., Pocovi, A., Millan, H., and Sussman, A.J., 2004, Map-view models for correcting and calculating shortening estimates in rotated thrust fronts using paleomagnetic data, *in* Sussman, A.J., and Weil, A.B., eds., Orogenic Curvature: Integrating Paleomagnetic and Structural Analyses: Geological Society of America Special Paper 383, p. 57–72.

Ramsay, J.G., 1981, Tectonics of the Helvetic nappes, *in* McClay, K.R., and Price, N.J., eds., Time and Place in Orogeny: London, Geological Society of London, p. 43–79.

Ries, A.C., and Shackleton, R.M., 1976, Patterns of strain variation in arcuate fold belts: Proceedings of the Royal Society of London, Series A, Mathematical and Physical Sciences, v. 283, p. 281–288, doi: 10.1098/rsta.1976.0085.

Royse, F., 1993, An overview of the geologic structure of the thrust belt in Wyoming, northern Utah, and eastern Idaho, *in* Snoke, A.W., Steidtmann, J.R., and Roberts, S.M. eds., Geology of Wyoming: Geological Survey of Wyoming Memoir 5, p. 272–311.

Royse, F., Warner, M.A., and Reese, D.L., 1975, Thrust belt structural geometry and related stratigraphic problems, Wyoming–Idaho–northern Utah, *in* Boylard, E.W., ed., Deep drilling frontiers of the central Rocky Mountains: Denver, Rocky Mountain Association of Geologists Symposium, p. 41–45.

Rubey, W.W., Oriel, S.S., and Tracey, J.I., Jr., 1980, Geologic Map and Structure Sections of the Cokeville 30-Minute Quadrangle, Lincoln and Sublette Counties, Wyoming: U.S. Geological Survey Map I-1129, scale 1:62,500.

Sans, M., Verges, J., Gomis, E., Pares, J.M., Schiattarella, M., Trave, A., Calvet, F., Santanach, P., and Coulcet, A., 2003, Layer parallel shortening in salt-detached folds: Constraints on cross-section restoration: Tectonophysics, v. 372, p. 85–104, doi: 10.1016/S0040-1951(03)00233-6.

Schill, E., Crouzet, C., Gautum, P., Singh, V.K., and Appel, E., 2002, Where did rotational shortening occur in the Himalayas? Inferences from palaeomagnetic remagnetizations: Earth and Planetary Science Letters, v. 203, p. 45–57, doi: 10.1016/S0012-821X(02)00842-7.

Schirmer, T.W., 1988, Structural analysis using thrust-fault hanging-wall sequence diagrams, Ogden duplex, Wasatch Range, Utah: American Association of Petroleum Geologists Bulletin, v. 72, p. 573–585.

Schwartz, S.Y., and Van der Voo, R., 1983, Paleomagnetic evaluation of the orocline hypothesis in the central and southern Appalachians: Geophysical Research Letters, v. 10, p. 505–508, doi: 10.1029/GL010i007p00505.

Schwartz, S.Y., and Van der Voo, R., 1984, Paleomagnetic study of thrust sheet rotation during foreland impingement in the Wyoming-Idaho Overthrust Belt: Journal of Geophysical Research, v. 89, p. 10,071–10,086.

Shimamoto, T., and Ikeda, Y., 1976, A simple algebraic method for strain estimation from deformed ellipsoidal objects: 1. Basic theory: Tectonophysics, v. 36, p. 315–337, doi: 10.1016/0040-1951(76)90107-4.

Speranza, F., Sagnotti, L., and Mattei, M., 1997, Tectonics of the Umbria-Marche-Romagna Arc (central northern Apennines, Italy): New paleomagnetic constraints: Journal of Geophysical Research, v. 102, p. 3153–3166, doi: 10.1029/96JB03116.

Stamatakos, J.A., Hirt, A.M., and Lowrie, W., 1996, The age and timing of folding in the Central Appalachians from paleomagnetic results: Geological Society of America Bulletin, v. 108, p. 815–829, doi: 10.1130/0016-7606(1996)108<0815:TAATOF>2.3.CO;2.

Suess, E., 1909, The Face of the Earth (translated from German by H.B.C. Sollas and W.J. Sollas): Oxford, Clarendon, 672 p.

Sussman, A.J., Butler, R.F., Dinares-Turell, J., and Verges, J., 2004, Vertical-axis rotation of a foreland fold: An example from the Southern Pyrenees: Earth and Planetary Science Letters, v. 218, p. 435–449, doi: 10.1016/S0012-821X(03)00644-7.

van der Pluijm, B.A., Craddock, J.P., Graham, B.R., and Harris, J.H., 1997, Paleostress in cratonic North America: Implications for deformation of continental interiors: Science, v. 277, p. 794–796, doi: 10.1126/science.277.5327.794.

Van der Voo, R., and Channell, J.E.T., 1980, Paleomagnetism in orogenic belts: Reviews of Geophysics and Space Physics, v. 18, p. 455–481, doi: 10.1029/RG018i002p00455.

Weil, A.B., and Sussman, A., 2004, Classification of curved orogens based on the timing relationships between structural development and vertical-axis rotations, *in* Sussman, A.J., and Weil, A.B., eds., Orogenic Curvature: Integrating Paleomagnetic and Structural Analyses: Geological Society of America Special Paper 383, p. 1–17.

Weil, A.B., Van der Voo, R., van der Pluijm, B.A., and Parés, J.M., 2000, Unraveling the timing and geometric characteristics of the Cantabria-Asturias Arc (northern Spain) through paleomagnetic analysis: Journal of Structural Geology, v. 22, p. 735–756, doi: 10.1016/S0191-8141(99)00188-1.

Weil, A.B., Van der Voo, R., and van der Pluijm, B., 2001, New paleomagnetic data from the southern Cantabria-Asturias Arc, northern Spain: Implications for true oroclinal rotation and the final amalgamation of Pangea: Geology, v. 29, p. 991–994, doi: 10.1130/0091-7613(2001)029<0991:OBAEAT>2.0.CO;2.

Weil, A.B., Yonkee, W.A., and Sussman, A.J., 2009, Reconstructing the kinematics of thrust sheet rotation: A paleomagnetic study of Triassic red beds from the Wyoming salient, U.S.A.: Geological Society of America Bulletin (in press).

Wilkerson, M.S., and Dicken, C.L., 2001, Quick-look techniques for evaluating two-dimensional cross sections in detached contractional settings: American Association of Petroleum Geologists Bulletin, v. 85, p. 1759–1770.

Wiltschko, D.V., and Dorr, J.A., 1983, Timing of deformation in overthrust belt and foreland of Idaho, Wyoming and Utah: American Association of Petroleum Geologists Bulletin, v. 67, p. 1304–1322.

Yonkee, W.A., 1992, Basement-cover relations, Sevier orogenic belt, northern Utah: Geological Society of America Bulletin, v. 104, p. 280–302, doi: 10.1130/0016-7606(1992)104<0280:BCRSOB>2.3.CO;2.

Yonkee, W.A., 2005, Strain patterns within part of the Willard thrust sheet, Idaho-Utah-Wyoming thrust belt: Journal of Structural Geology, v. 27, p. 1315–1343, doi: 10.1016/j.jsg.2004.06.014.

Yonkee, W.A., DeCelles, P.G., and Coogan, J.C., 1997, Kinematics and synorogenic sedimentation of the eastern frontal part of the Sevier orogenic wedge, northern Utah, *in* Link, P.K., and Kowallis, B.K., eds., Proterozoic to Recent Stratigraphy, Tectonics, and Volcanology, Utah, Nevada, Southern Idaho, and Central Mexico: Brigham Young University Studies, v. 42, p. 355–380.

Manuscript Received 13 June 2008
Revised Manuscript Received 31 December 2008
Manuscript Accepted 5 January 2009

Printed in the USA